communications earth & environment

Article

A Nature Portfolio journal

https://doi.org/10.1038/s43247-025-02965-z

Accelerating sea level rise in Africa and its large marine ecosystems since the 1990s

Franck Eitel Kemgang Ghomsi [1,2,3] ✉, Julienne Stroeve [1,4,5], Antonio Bonaduce [6] & Roshin P. Raj [6]

Sea-level rise poses a significant threat to Africa's vital coastal ecosystems and the livelihoods of its growing populations. Here we analyze 31 years of satellite altimetry data to quantify sea-level change across Africa's Large Marine Ecosystems, vast ocean regions of high biological productivity. The rate of rise has accelerated markedly to 4.34 mm/yr since 2010, over four times the 1990s rate. This is primarily driven by two factors: an increase in ocean mass from melting ice sheets accounts for over 80% of the total rise, with the remainder reflecting the expansion of warming ocean water. Regional rates are fastest in the Red Sea and Guinea Current, while increased salinity suppresses the trend in the Mediterranean. 2023 was particularly severe, with record-high sea levels across nearly 40% of Africa's surrounding ocean. This uneven rise intensifies risks for over 50 million coastal residents, underscoring the urgent need for region-specific adaptation.

Sea-level rise (SLR) stands among the most visible and rapidly accelerating consequences of anthropogenic climate change, posing an escalating threat to coastal systems globally. Manifesting through chronic flooding, shoreline erosion, saltwater intrusion, and the degradation of critical ecosystems, SLR has far-reaching consequences for both biodiversity and human livelihoods[1,2]. Since 1993, satellite altimetry missions including TOPEX/Poseidon, the Jason series, and Sentinel-6, have documented a persistent rise in global mean sea level (GMSL), currently estimated at 3.4 ± 0.3 mm/yr with an acceleration of 0.12 ± 0.05 mm/yr[2–4]. This increase is attributed to thermal expansion, along with ice mass loss from polar regions, glacier retreat and terrestrial water storage changes[5,6]. In 2023, ocean heat content in the upper 100 m reached unprecedented levels, with Marine heatwaves affecting up to 40% of the global ocean that further intensified steric contributions to sea level and exacerbated coastal vulnerabilities[7,8].

While SLR is a global phenomenon, its impacts are profoundly uneven and nowhere is this inequity more pronounced than in Africa (40°S–40°N, 25°W–60°E). Despite contributing to less than 4% of global CO_2 emissions, the continent bears a disproportionate burden of climate-related risks that threaten socio-economic stability, ecological integrity, and cultural heritage[9–11]. Africa's 40,000-km coastline supports over 250 million people (Fig. 1), many of whom reside in low-lying urban centers like Alexandria, Cape Town, Dar es Salaam, Douala, and Lagos[12,13]. These cities are increasingly exposed to recurrent flooding, coastal erosion, and saltwater intrusion[14–17]. Moreover, local processes such as land subsidence and aquifer over-extraction amplify the effects of global SLR. In Lagos, for instance, subsidence rates of 8–12 mm/yr driven by intensive groundwater withdrawal significantly magnify relative SLR[18–20].

The fragility of Africa's coasts is further exacerbated by the deteriorating condition of its marine ecosystems. Africa's seven Large Marine Ecosystems (LMEs) the Mediterranean, Red Sea, Somali Coastal Current, Agulhas Current, Benguela Current, Guinea Current, and Canary Current are ecological and economic lifelines that support diverse marine life and critical ecosystem services. However, these LMEs are under mounting pressure from both climate and anthropogenic stressors, including unregulated development, dam-induced sediment trapping, and habitat degradation[21,22]. Natural buffers like mangroves, coral reefs, and wetlands are steadily eroded, diminishing coastal resilience. At the same time, many African countries lack the infrastructure, early warning systems, and financial resources needed for adaptation[23,24].

These vulnerabilities are particularly acute in Eastern Boundary Upwelling Systems (EBUS) such as the Benguela and Canary Currents, which are among the world's most productive marine systems[22]. These regions play an essential role in fisheries and climate regulation but are increasingly threatened by rising ocean temperatures, vertical stratification, and declining nutrient fluxes, all of which compromise marine productivity[21,22,25,26]. Meanwhile, non-EBUS regions, including the Somali and Guinea Currents, remain poorly studied despite their ecological and socio-economic importance. This highlights a critical knowledge gap that undermines effective adaptation planning in these regions. Island nations like Cape Verde, Seychelles, and São Tomé face even greater existential

[1]Centre for Earth Observation Science, University of Manitoba, Winnipeg, MB, Canada. [2]Department of Oceanography, University of Cape Town, Cape Town, South Africa. [3]Geodesy Research Laboratory, National Institute of Cartography, Yaoundé, Cameroon. [4]Department of Earth Sciences, University College London, London, UK. [5]National Snow and Ice Data Center, Cooperative Institute for Research in Environmental Science, University of Colorado Boulder, Boulder, CO, USA. [6]Nansen Environmental and Remote Sensing Center and Bjerknes Center for Climate Research, Bergen, Norway. ✉e-mail: franckeitel@gmail.com; franck.kemgangghomsi@umanitoba.ca

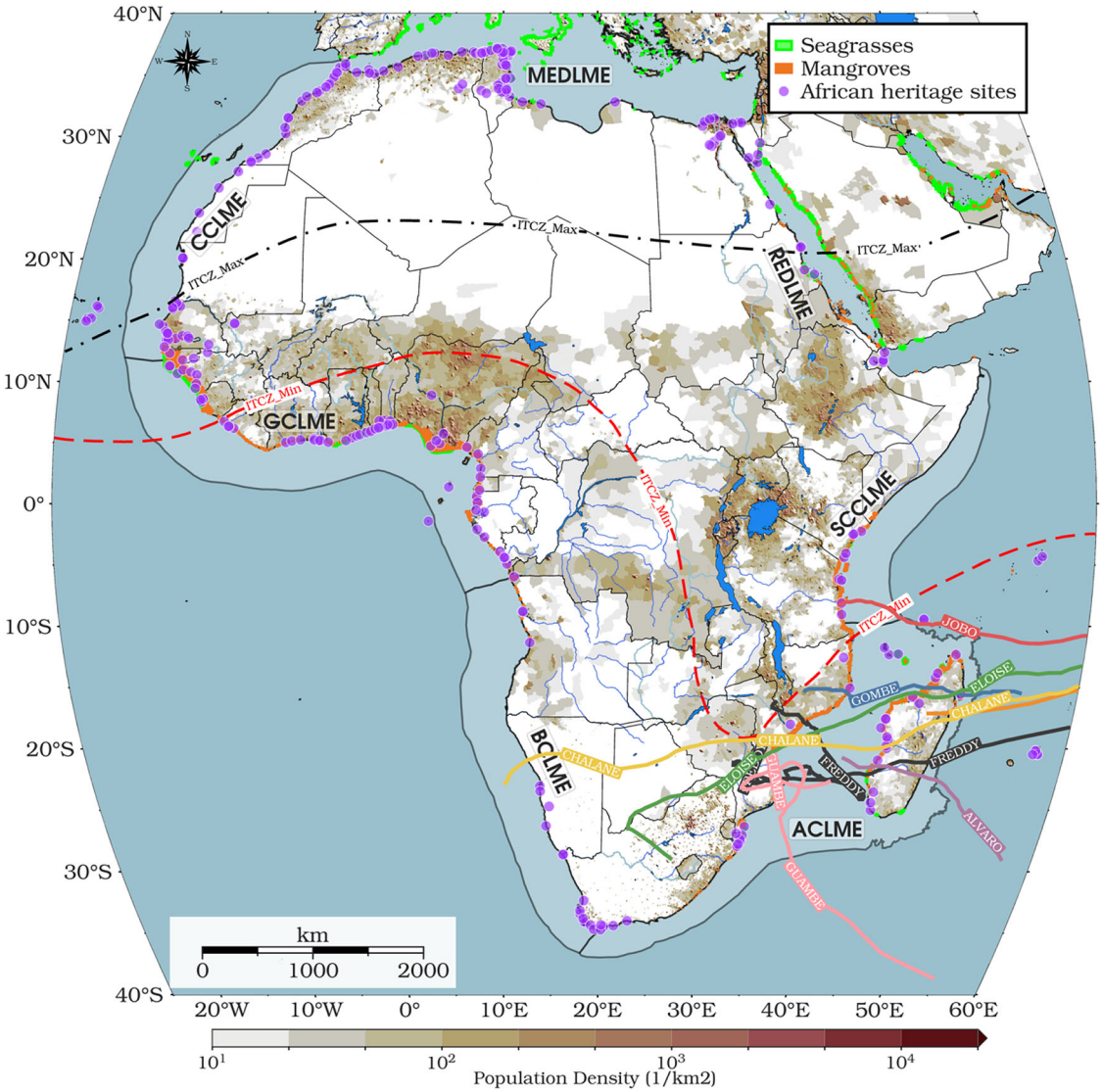

Fig. 1 | Coastal vulnerabilities and oceanographic context of Africa. Population distribution across Africa, overlaid with the tracks of major tropical cyclones that have severely impacted East and Southern Africa over the past seven years: Alvaro (April 2019), Chalane (December 2020), Eloise (January 2021), Guambe (February 2021), Jobo (April 2021), Gombe (March 2022), and Freddy (February–March 2023). Solid lines indicate cyclone paths, while red and black dashed lines represent the minimum and maximum seasonal positions of the Intertropical Convergence Zone (ITCZ), marking the extent of the African monsoon. The boundaries of Africa's seven LMEs are delineated in bold, ordered from highest to lowest annual ecosystem service value: Agulhas Current (ACLME, NOAA ID: 30), Red Sea (REDLME, 33), Somali Coastal Current (SCCLME, 31), Benguela Current (BCLME, 29), Guinea Current (GCLME, 28), Canary Current (CCLME, 27), and Mediterranean (MEDLME, 26), based on NOAA's classification (https://www.st.nmfs.noaa.gov/ecosystems/lme/). Africa's heritage location sites are marked with purple dots.

threats. With limited land area and economies closely tied to the ocean, they are especially vulnerable to the climate-related impacts of coral bleaching[27,28], intensified storm surges, and shoreline retreat. The first two impacts are largely driven by ocean warming, whereas the third impact is a product of human intervention in coastal processes and SLR. These island states serve as stark microcosms of broader continental challenges, highlighting the urgency of regional SLR research.

Compounding these regional vulnerabilities are large-scale climate oscillations and extreme weather events. The West African Monsoon (WAM), governed by the seasonal movement of the Intertropical Convergence Zone (ITCZ), delivers intense rainfall to the coastal zone, particularly the Gulf of Guinea[29,30]. Since 2000, the WAM has intensified, with a 15–20% increase in extreme rainfall events (≥85 mm/day), often resulting in devastating floods[31]. In 2023, a strong El Niño event caused a northward shift of the ITCZ, bringing unusually heavy rainfall and displacing over a million people in Cameroon, Ghana, Nigeria, and neighboring countries[32,33]. These events further exacerbate the compound nature of SLR and extreme rainfall, which together undermine the resilience of coastal communities[15,34,35].

Tropical cyclones and their associated storm surges further intensify the threat. Events such as Cyclone Eloise (2021), Tropical Storm Ana (2022), Cyclone Freddy (2023), and Storm Daniel (2023) have collectively affected more than 4 million people across Mozambique, Malawi, and Libya, with devastating consequences[3,36,37] (Fig. 1). These rising seas are growing in frequency and intensity, outpacing the adaptive capacities of vulnerable nations. Notably, the 2023 failure of Libya's Derna Dam during Storm Daniel was triggered by exposed structural vulnerabilities despite precipitation levels being within the dams' design limits[38]. The destruction of Libya's Derna Dam serves as a sobering reminder of the need for integrated, forward-looking disaster risk strategies.

Understanding and projecting regional sea-level trends requires disentangling their physical components. Total SLR results from both steric (density-driven) and manometric (mass-driven) changes, with steric SLR subdivided into thermosteric (temperature-induced) and halosteric

(salinity-induced) contributions[39]. In the Eastern Tropical Atlantic, recent studies show thermosteric contributions of 0.56 ± 0.03 mm/yr and ocean mass contributions of 2.66 ± 0.50 mm/yr[14]. However, halosteric trends, particularly in Africa's LMEs, remain poorly constrained, limiting the accuracy of regional projections and adaptation planning. Further cloaking regional assessments are remote climate drivers. Teleconnection patterns such as the El Niño–Southern Oscillation (ENSO), the Indian Ocean Dipole (IOD), the Tropical Atlantic SST Index (TASI), and the North Atlantic Oscillation (NAO) modulate sea-level anomalies by influencing ocean circulation, vertical mixing, and thermal stratification[7,14]. The 2023 El Niño event, for example, not only amplified regional sea-level anomaly (SLA) variability but also intensified mean sea levels[40,41], underscoring the importance of incorporating these remote signals into regional assessments.

Despite the mounting risks, Africa remains underrepresented in global sea-level research. Most studies focus on global aggregates or select regions, particularly EBUS, leaving large portions of the African coastline unstudied. This uneven distribution of knowledge perpetuates an adaptation gap, undermining resilience in some of the world's most vulnerable regions[42,43]. This underrepresentation highlights the urgent need for targeted studies across the entire African coastline.

Drawing on three decades of satellite altimetry data from 1993 to 2023, this study aims to: (a) conduct an in-depth analysis of the record-breaking year 2023; (b) quantify updated SLA trends and disentangle the sea-level budget into the respective contributions of steric components (thermosteric and halosteric) and ocean mass, while incorporating Glacial Isostatic Adjustment (GIA) corrections; and (c) evaluate the influence of interannual climate modes on regional sea-level variability across Africa and its LMEs. By expanding the analysis beyond EBUS to include underrepresented LMEs and island nations, this study provides the first holistic synthesis of relative SLR dynamics across the African continent. In doing so, it addresses a critical gap in sea-level science and offers a robust foundation for evidence-based coastal planning and climate resilience.

Results

Regional sea level rise and the exceptional 2023 event in Africa

Long-term acceleration in African sea level rise (1993–2023). Satellite altimetry shows Africa's regional mean geocentric sea level (RMSL) rose by 10.25 cm from 1993 to 2023, driven by a linear trend of 3.31 ± 0.04 mm/yr and an acceleration of 0.11 ± 0.02 mm/yr² (GIA-corrected; see Fig. 2a). Vertical land motion, while influencing relative SLR, does not affect altimetry-derived geocentric trends. This acceleration is comparable to the global rate (0.12 ± 0.05 mm/yr²)[3,44]. Notably, 2023 recorded the highest annual mean sea level to date. This increase is statistically significant, with a trend difference of 3.39 mm/yr between the first and last decades, and a notable 1.41 mm/yr difference between the last two decades (2003–2012 vs. 2013–2023). The rate of SLR

has sharply increased, with cumulative SLRs (i.e., total increases over each decade) of approximately 0.92 cm (1993–2002), 2.82 cm (2003–2012), and 4.60 cm (2013–2023). The rate rose from 0.96 ± 0.26 mm/yr in the first decade to 4.34 ± 0.18 mm/yr in the last, a 4.54 ± 1.26-fold increase (Fig. 2a). Over the past two decades, the average rate (3.67 ± 0.16 mm/yr) was 1.2 times the long-term trend, highlighting ongoing acceleration since the early 1990s (Supplementary Fig. 1).

This acceleration reflects intensified contributions from thermal expansion due to ocean warming and increased individual mass contributions, including glacier melt, Greenland and Antarctic ice sheets, changes in land water storage, freshwater fluxes, and atmospheric water vapor content[45]. These regional changes coincide with a globally coherent climate shift that began in the early 2010s, as evidenced by synchronized transitions in oceanic and atmospheric parameters worldwide, further underscoring the systemic nature of the observed SLR[44]. This rise is further amplified by mass contributions from melting glaciers, Greenland and Antarctic ice sheets, and changes in land water storage[46,47], as depicted in the trend curve of Fig. 2a. While the long-term trend is generally upward, it includes minor fluctuations—for example, a subtle 0.09 cm decrease between 2021 to 2022 (ranking 22nd among 31 annual changes), likely influenced by regional ocean circulation anomalies. This was followed by a rise of 1.97 cm from 2022 to 2023—the second-highest annual increase on record, surpassed only by the 1997–1998 El Niño-driven rise. This increase drove 2023 to the highest annual domain-averaged SLA of 10 cm, with peak monthly values in November (12.50 cm) and December (12.73 cm) ranking as the top two months over the 1993–2023 period (see Supplementary Fig. 2). Notably, the 2022–2023 increase significantly outpaced the global mean rise of 0.59 cm.

Complementing the temporal evolution, the spatial patterns in 2023 reveal an alarming extent of regional SLAs. Spatially, more than 95% of the African ocean surface exhibited elevated sea levels in 2023 compared to the 1993–2022 climatology — here defined as the average sea level over that 30-year period (Fig. 2b)—with more than 75% showing an increase relative to 2022. In 2023, monthly SLAs across Africa and its seven LMEs significantly exceeded the 1993–2022 climatology, with differences of 4.22–8.53 cm for Africa and up to 16.24 cm for the Somali Coastal Current (December). Other LMEs, including the Guinea Current (up to 8.67 cm, June), Benguela Current (up to 8.36 cm, December), and Mediterranean Sea (up to 11.22 cm, May), showed anomalies of 2.82–11.22 cm (Supplementary Fig. 2). Notably, 1.5% of the region experienced rises exceeding 10 cm, particularly in dynamic ocean systems such as the Agulhas Current (Fig. 2c). These localized hotspots of SLR are consistent with areas of strong mesoscale activity and boundary currents. By 2023, 38.6% of the regional ocean, especially in the Eastern Tropical Atlantic, reached its highest annual sea level on record, while 72.1% recorded peak levels during or after 2020 (Fig. 2d). This clustering of record-high sea level years since 2020 confirms that recent intensification is not isolated but rather part of a sustained spatial trend affecting large portions of the basin. This widespread occurrence of record-high sea levels in recent years points to a sustained and intensifying trend. These patterns align with global sea level trends, which show a 10.5 cm rise over the same period, but the accelerated rates and extreme annual increases in the African region amplify risks for coastal communities. The widespread elevation, affecting 95.8% of the region, underscores heightened coastal flooding risks, particularly in the Somali and Guinea Currents (Fig. 2b–d). These areas face heightened threats of inundation, salinization of freshwater resources, and loss of critical ecosystems.

Peak SLA years and the exceptional 2023 event. We assessed annual mean and peak monthly SLA, as well as their residuals, after removing the 1993–2023 GMSL trend (3.4 ± 0.3 mm/yr), as shown in the residuals time series in Fig. 3a. The analysis focused on five peak years: 1995, 1997, 2010, 2019, and 2023. Residuals were calculated by subtracting a linear GMSL trend fitted to satellite altimetry data for the African region, isolating spatially variable anomalies driven by regional oceanographic or climate processes. Peak months were identified as the months with the highest SLA per year. Notably, the 2023 values were exceptional. The annual mean SLA reached 67.95 mm, which was 19.24 mm higher than in 2019, and the December peak month SLA reached 77.65 mm, significantly exceeding 2019's 56.66 mm, as illustrated in Fig. 3b. After removing the GMSL trend, the 2023 residuals remained outstanding: annual mean residuals were 14.13 mm, the highest of all years, and peak month residuals reached 22.32 mm, surpassing 1997's value by 24.9%. Statistical tests, including Bonferroni-corrected t-tests[48] ($p < 0.0125$ for 1997, 2010, 2019), supported the presence of persistent, regionally coherent anomalies, likely reflecting steric (temperature- and salinity-driven) or circulation-driven variability. Fig. 3b summarizes these metrics across peak years, underscoring 2023's exceptional ranking in all categories and highlighting 2023's dominance across all four metrics. Consequently, 2023 stands apart from years like 1997, which exhibited large residuals (16.64 mm) linked to the 1997–1998 El Niño, and 2019 Atlantic Niño, which showed high SLA (56.66 mm) but smaller residuals (14.53 mm). Trend analysis further supports this conclusion: SLA trends accelerated

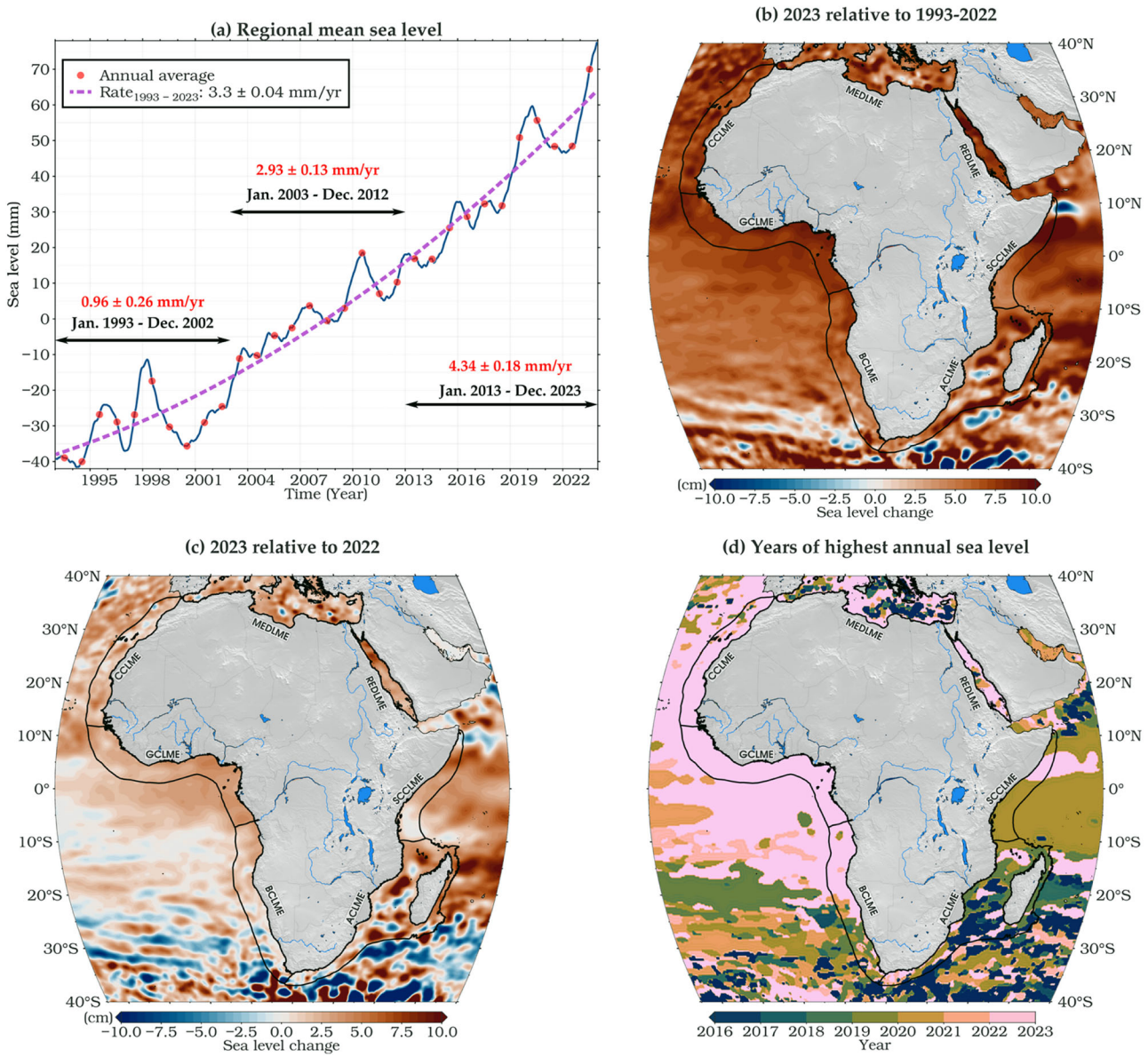

Fig. 2 | Regional sea level variability and anomalies across Africa (1993–2023). **a** Time series of regional monthly mean sea level for Africa derived from satellite altimetry. Annual means are shown by red markers, with a purple curve representing a second-order polynomial trend. **b** Annual mean sea level for 2023 expressed as anomalies relative to the 1993–2022 baseline. **c** Difference between 2023 and 2022 annual means. **d** Spatial distribution of the year with the peak annual sea level recorded during the altimetry period. In 2023, sea levels across much of Africa continued to rise, primarily driven by global warming and modulated by large-scale climate variability such as El Niño. The seven African LMEs are labeled as in Fig. 1.

over the three decades, providing context for the residuals in Fig. 3a. This acceleration, combined with 2023's large residuals, suggests contributions from both global and regional drivers, potentially linked to basin-scale climate variability, such as the 2023–2024 El Niño/Atlantic Niño or changes in coastal circulation. However, further analysis is needed to confirm these mechanisms. In conclusion, 2023 represents the most extreme regional SLA event in the satellite record for Africa, characterized by unprecedented magnitude, persistence after global signal removal, and strong regional forcing atop an accelerating background of global SLR.

Sea levels trends and its components

Regional trends variability. In this section, we analyze the spatial and long-term trend of the total SLA from 1993 to 2023, based on a reanalysis dataset that integrates altimetric, thermosteric, halosteric, and manometric components. This comprehensive approach captures the combined influence of these factors on sea level variability across the African region and its LMEs. We also quantify the relative contributions of the total steric effect and its individual components to overall sea level variability. As illustrated in Fig. 4a, the SLA trend map reveals significant spatial patterns, with a statistically significant ($p < 0.05$) trend in the RMSL. The color gradient (from blue to yellow) reflects the global mean SLR of 3.4 ± 0.3 mm/yr over the same period shown as a gray contour, which is used as a reference threshold[44,49] to distinguish areas experiencing below- or above-average SLR compared to the global mean. Although the regional mean rate is similar to the GMSL, this average mask substantial spatial heterogeneity. Fig. 4a shows that much of the African oceanic region experiences sea-level anomaly (SLA) trends above the GMSL, particularly across several LMEs. Notably, the Guinea Current (GCLME), Canary Current (CCLME), Red Sea (REDLME), Somali Coastal Current (SCCLME), and the northern parts of the Benguela Current (BCLME) and Agulhas Current (ACLME) exhibit SLR rates

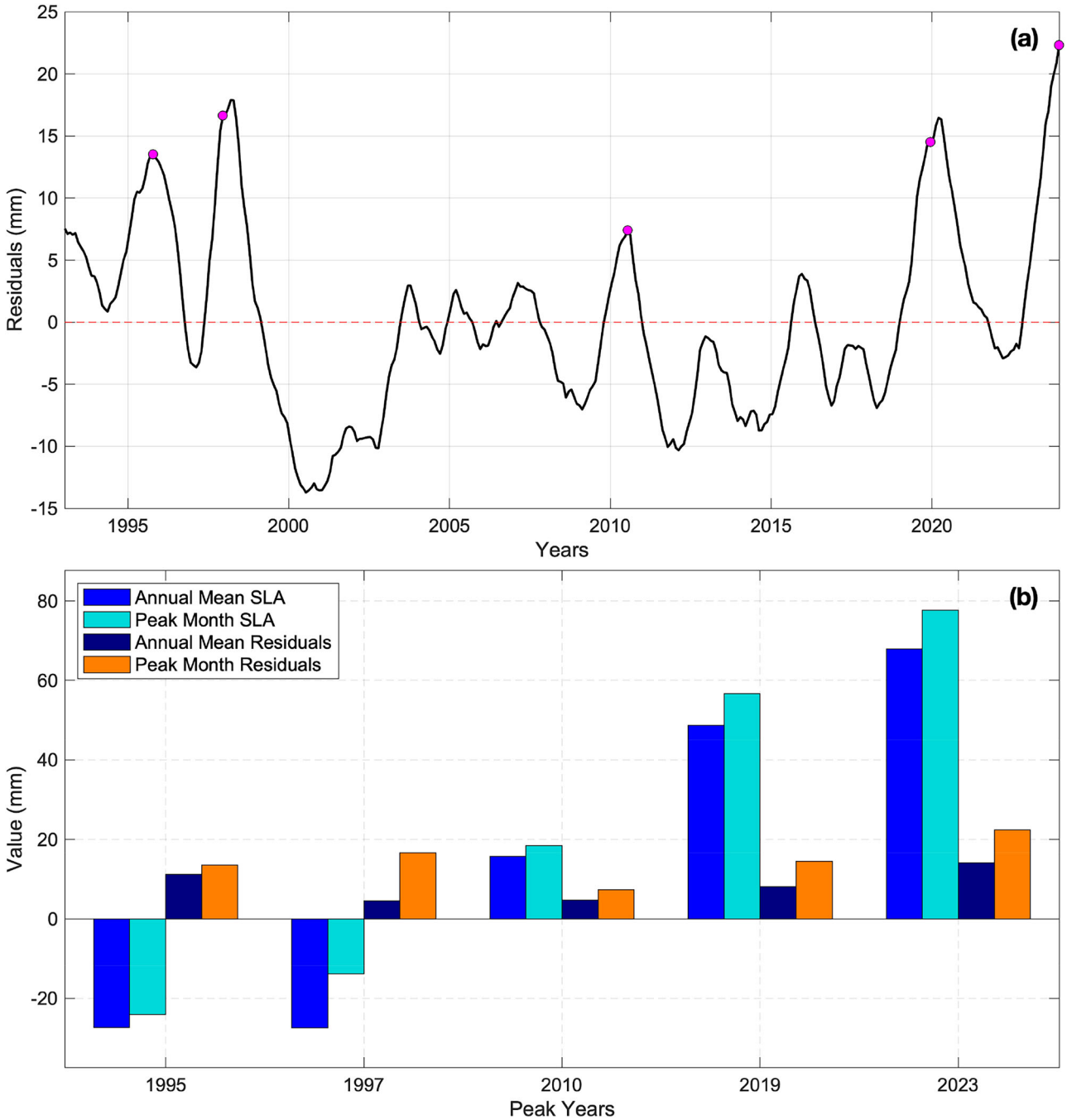

Fig. 3 | Residual sea level anomalies in Africa highlight the exceptional nature of 2023. a Time series of SLA residuals after removing the 1993–2023 GMSL trend, with pink dots marking peak maxima. **b** Comparison of SLA and residual magnitudes for selected peak years. The year 2023 exhibits the largest anomalies in both SLA and residuals across the satellite record, persisting even after global trend removal.

exceeding the GMSL. These elevated rates may be linked to intensified wind-driven circulation or enhanced tropical thermosteric expansion. In contrast, the Mediterranean LME (MEDLME) (see Fig. 1) shows trends below the global mean.

The trends in SLA across Africa's seven LMEs, as shown in Fig. 4a, reflect a compound interplay between steric (thermosteric + halosteric) and manometric components, each contributing differently across regions. These components interact to create distinct spatial patterns in SLA, shaped by both local and large-scale oceanographic processes. In the equatorial and tropical LMEs-such as the GCLME, CCLME, SCCLME, and the REDLME-thermosteric expansion, driven by ocean warming, is the principal contributor to SLR. The steric component, which encompasses changes in seawater density due to temperature and salinity, accounts for 19.78% of the total SLA in the entire region, as depicted in Fig. 4b. Notably, the thermosteric signal alone contributes 27.90% of SLA and exceeds the total steric trend by 41.10% (see Fig. 4c), underscoring the dominant role of thermal expansion. This effect is especially pronounced along the equatorial Atlantic and Indian Ocean margins, where persistent high temperatures and seasonal upwelling fuel significant thermal expansion.

In contrast, subtropical regions such as the MEDLME display different dynamics. In the CCLME, thermosteric trends closely mirror SLA patterns, indicating that temperature-driven expansion remains important, as shown in Fig. 4a and Fig. 5 However, in the MEDLME, SLA variability aligns more closely with halosteric changes—those driven by salinity-evident in Fig. 4d. The halosteric signal strongly influences sea level trends in the MEDLME, where increased evaporation and reduced freshwater input elevate salinity,

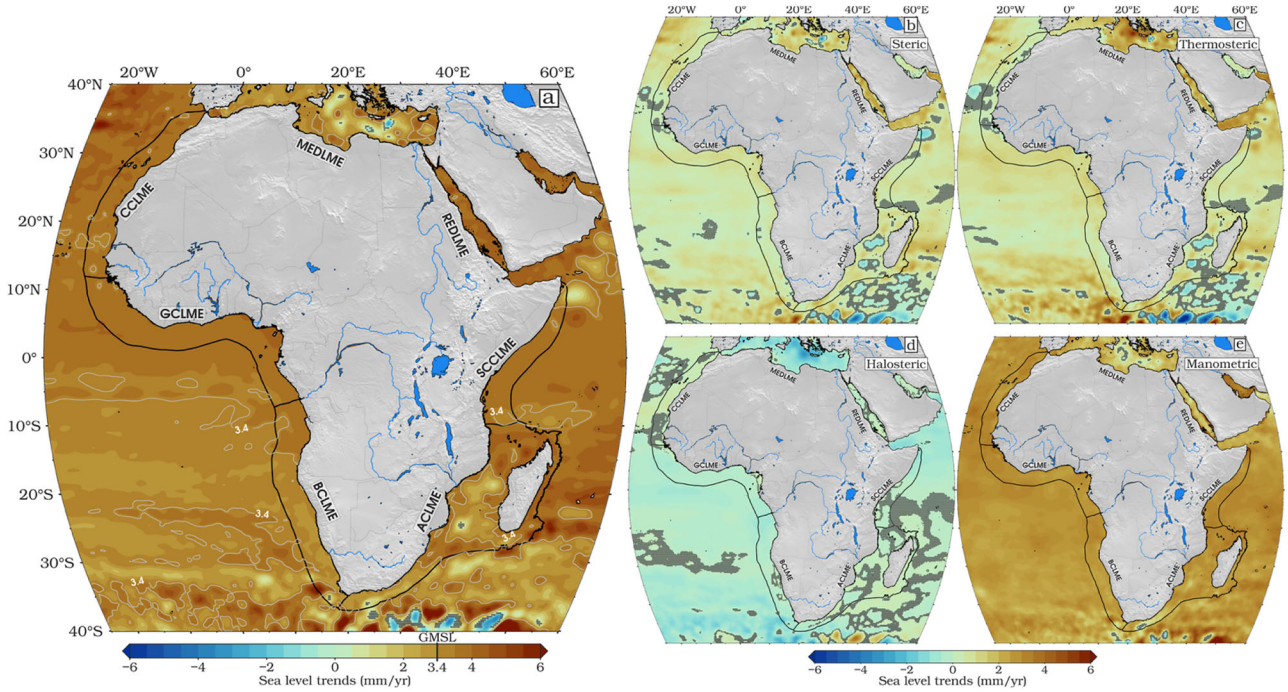

Fig. 4 | Spatial distribution of regional sea-level trends across Africa's coastal LMEs from 1993 to 2023. a Total sea-level trend; **b** total steric; **c** thermosteric; **d** halosteric; and **e** manometric (SLA minus steric) trends. GIA corrections were applied to both SLA and manometric trends. At each grid point, mean and seasonal cycles were removed prior to trend estimation. All trends are statistically significant at the 95% confidence level except in areas marked with gray dots. The seven African LMEs are labeled as in Fig. 1.

making it the dominant steric driver. The halosteric component, on average, exerts a modest but negative influence on SLA across most LMEs, contributing −8.13% (Fig. 4d). Negative halosteric trends are most notable in the MEDLME and broader North BCLME at the Congo River runoffs, likely linked to regional climate and hydrological patterns. Positive halosteric trends are mostly observed in the CCLME and ACLME, with localized positive trends in the GCLME, particularly off the coasts of Cameroon and Liberia, where major rivers discharge freshwater into the ocean, as highlighted in Fig. 4d. These regions, along with parts of the REDLME, Agulhas retroflection zone, and ACLME, experience enhanced steric SLR due to reduced water column density from riverine and estuarine runoff. Such freshwater inputs and regional circulation changes can locally offset the broader negative halosteric trend, highlighting the importance of hydrological variability in shaping regional sea level patterns. Dominating the SLA signal is the manometric component, which accounts for 80.23% of the total trend, as illustrated in Fig. 4e. Manometric sea level changes refer to variations caused by the redistribution of ocean mass, primarily from land ice melt, changes in terrestrial water storage, and large-scale shifts in the global water cycle. These changes are measured as the difference between total sea level changes (from satellite altimetry) and steric changes (from in situ temperature and salinity observations). In Africa, manometric trends generally range between 1.8 and 2.9 mm/yr in most LMEs. The highest values are observed in the SCCLME and GCLME, while lower rates (0.5–2 mm/yr) occur in the southernmost ACLME, MEDLME, and REDLME (Fig. 4e).

Figure 5a provides a comprehensive view of SLR trends over Africa by illustrating the evolution of the total SLA and its contributing components. The SLA (depicted by the blue line) shows a steady and significant upward trend of 3.30 ± 0.04 mm/yr since the early 1990s, closely aligning with the GMSL trend of 3.4 mm/yr. As shown in Fig. 5b, this regional trend masks a pronounced acceleration, increasing from 0.96 ± 0.26 mm/yr in 1993–2002 to 4.34 ± 0.18 mm/yr in 2013–2023, a more than fourfold increase, driven by two primary processes: steric changes, due to variations in seawater density (temperature and salinity), and manometric changes, linked to shifts in ocean mass from cryospheric and hydrological processes. The manometric contribution (orange line, Fig. 5a), with a trend of 2.61 ± 0.04 mm/yr, accounts for 79% of the SLA rise, dominating the total SLR. This is in line with Bellas-Manley et al.[50], who found that the rise is primarily driven by mass inputs from global ice melt, especially Antarctic ice loss, which contributes up to 1.2 mm/yr through gravitational fingerprints in southern LMEs and Greenland's more uniform effect, alongside changes in land water storage[51]. Manometric contributions have accelerated significantly, rising by 3.28 ± 0.11 mm/yr above 1993–2002 (Fig. 5b) levels, underscoring their pivotal role in shaping regional sea-level patterns. This acceleration closely tracks the intensified glacier melt reported by Dussaillant et al.[52] with five of the last six years (2019, 2020, 2022, 2023, and 2024) exceeding 430 Gt/yr, reinforcing the substantial contribution of glaciers to the SLR acceleration observed along African coasts. The post-2019 period of exceptional melt coincides with the smaller, but still positive, increment in manometric acceleration from the second to the third decade, indicating that while the largest step-change occurred earlier (1993–2002 to 2003–2012), sustained high rates of glacier and ice-sheet loss in recent years have maintained and reinforced elevated mass-driven SLR trends across African LMEs. GIA has a negligible impact (<0.1 mm/yr) on African coasts, far from past ice sheet collapse regions. In contrast, the steric contribution (green line, Fig. 5a) is minor, with a trend of 0.34 ± 0.02 mm/yr, reflecting changes in seawater density. This is subdivided into thermosteric (temperature-driven) and halosteric (salinity-driven) components. The thermosteric anomaly (red line) exhibits a positive trend of 0.49 ± 0.02 mm/yr, indicating that ocean warming and thermal expansion are significant within the steric component. Conversely, the halosteric anomaly (purple line) shows a negative trend of −0.15 ± 0.01 mm/yr, suggesting that increasing salinity slightly counteracts SLR by increasing seawater density. The higher thermosteric trend compared to the total steric trend indicates that the halosteric component modestly offsets warming effects. While steric changes drive interannual variability, the manometric component, significantly driven by glacier melt as quantified by Dussaillant et al.[52] dominates the accelerated SLR affecting African coastal regions.

Figure 5 clarify the relative contributions, highlighting the dominance of the manometric component, followed by the thermosteric contribution,

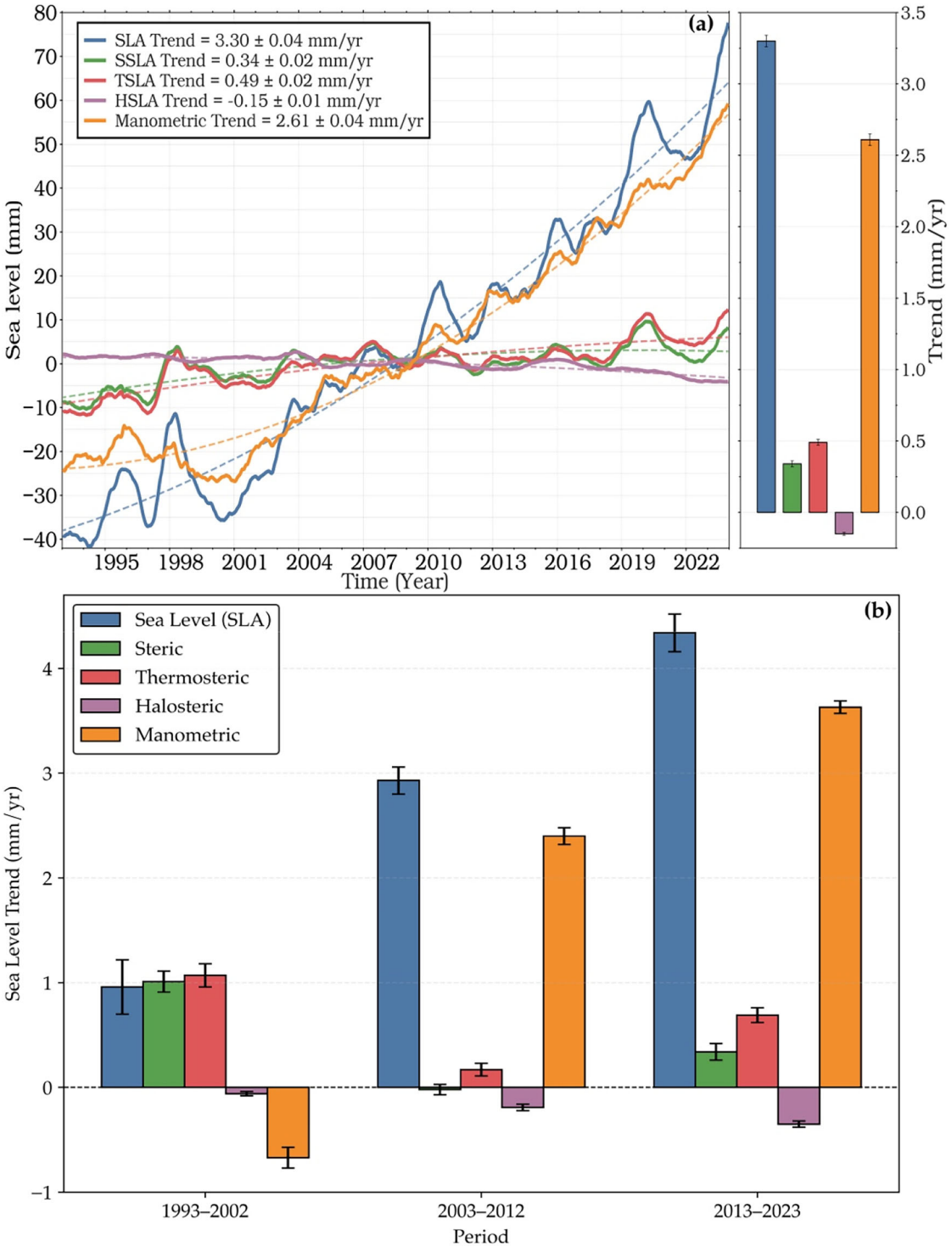

Fig. 5 | Temporal evolution and decadal sea level components for Africa. a Time series and linear trends of de-seasoned monthly anomalies of total SLA (blue), steric (SSLA; green), thermosteric (TSLA; red), halosteric (HSLA; purple), and manometric (orange) components from 1993 to 2023. Trend values for each component are indicated. All time series are smoothed using a 13-month low-pass filter to highlight interannual-to-decadal variability. **b** Decadal sea-level trends and component contributions for the African region, with bars showing trends (mm yr^{-1}) and error bars indicating uncertainties.

with the halosteric effect remaining negative and minor. All components exhibit temporal variability, with short-term oscillations superimposed on long-term trends.

As shown in Fig. 5b, the African oceanic domains exhibit an increased trend over the observed last two decades, with the most recent decade marking an unprecedented increase in sea level, a signature of the strongest acceleration recorded to date. This regime shift aligns with the peak glacier mass loss documented by Dussaillant et al.[52] particularly the 2023 record of 540 ± 69 Gt, contributing 1.5 mm to GMSL rise, which exacerbates regional SLR impacts on African coasts through enhanced ocean mass inputs. The steric components, in particular, show notable interannual variability, likely linked to climate phenomena such as ENSO and shifts in the ITCZ, which influence temperature and salinity distributions in the tropical ocean. Africa LMEs Sea level trends.

Atlantic Ocean LMEs. The CCLME, a productive eastern boundary upwelling system situated along northwest Africa in the Atlantic Ocean, exhibits a SLA trend of 3.30 ± 0.05 mm/yr over the study period Fig. 6a). This rise is primarily driven by mass (manometric) contributions of 2.63 ± 0.05 mm/yr, accounting for approximately 80% of the total and largely attributable to intensified land ice melt[39,45]. Steric contributions (0.66 ± 0.04 mm/yr), comprising about 20% of the SLA, include modest thermosteric expansion (0.47 ± 0.06 mm/yr) and a smaller positive halosteric signal (0.19 ± 0.03 mm/yr), the latter reflecting a salinity decrease primarily driven by increased continental runoff and possibly changes in precipitation, which overwhelms the salinizing effect of evaporation[53,54]. As a productive upwelling zone, the CCLME experiences moderated upper-ocean warming due to the persistent influx of cooler, nutrient-rich subsurface waters, which temper thermosteric expansion[25,55]. This upwelling-related cooling becomes more apparent in the decadal evolution of sea level trends. Between 1993–2002 (Fig. 9, Supplementary Table 1), SLA rose at 3.12 ± 0.30 mm/yr, driven largely by strong thermosteric expansion (2.07 ± 0.32 mm/yr). SLA peaked at 4.61 ± 0.31 mm/yr in 2003–2012, coinciding with an exceptional thermosteric contribution of 4.08 ± 0.23 mm/yr. However, in the most recent decade (2013–2023), although the SLA further increased to 4.69 ± 0.18 mm/yr, the thermosteric contribution dropped sharply to 0.45 ± 0.16 mm/yr—a decline of 1.60 mm/yr from the 1993–2002 (Fig. 9a) level-consistent with enhanced upwelling reducing heat retention in the upper ocean[55]. In parallel, mass contributions nearly doubled from 1.39 ± 0.18 mm/yr in 1993–2002 (Figs. 9a) to 3.12 ± 0.10 mm/yr in 2013–2023 (Fig. 9c), underscoring the increasing influence of land ice melt. Halosteric trends also shifted markedly from negative (−0.35 ± 0.04 mm/yr) to positive values (1.12 ± 0.07 mm/yr), reflecting a transition from salinity increase (which raises density and contributes negatively to sea level) to salinity decrease (which lowers density and contributes positively). This shift likely reflects enhanced freshwater input[53]. This shift supported a steric contribution of approximately 33% in the latest decade, with halosteric effects playing a more prominent role.

Bordering the West African coast, the GCLME spans approximately 2 million km² and is characterized by seasonal upwelling, high freshwater input, and low-salinity surface waters[25,56]. Between 1993 and 2023, this region experienced a SLA trend of 3.41 ± 0.05 mm/yr, slightly above the global mean ranking it second among all LMEs (Fig. 6b).

This rise is predominantly driven by mass (manometric) contributions of 2.68 ± 0.03 mm/yr, representing about 79% of the total. Steric effects contribute 0.72 ± 0.04 mm/yr (21%) to the regional sea level trend in the GCLME. Of this, thermosteric expansion estimated at 1.07 ± 0.05 mm/yr reflects upper-ocean warming across the tropical Atlantic, amplified by seasonal upwelling that redistributes heat in the upper layers, while halosteric changes (−0.35 ± 0.02 mm/yr) indicate contraction driven by salinity increase (i.e., density increase causing volume reduction). These findings align with recent studies emphasizing the joint role of mass and steric components in driving SLR in river-dominated tropical LMEs[57]. A decadal breakdown reveals a marked acceleration: SLA increased from 2.00 ± 0.27 mm/yr in 1993–2002 (Fig. 9a) to 4.50 ± 0.19 mm/yr in 2013–2023 (Fig. 9c), a 2.25-fold rise. Initially, this was supported by modest contributions from mass (0.54 ± 0.11 mm/yr) and thermosteric (1.55 ± 0.30 mm/yr) components. During 2003–2012 (Fig. 9b), both peaked, with manometric input reaching 3.63 ± 0.11 mm/yr and thermosteric expansion at 1.41 ± 0.18 mm/yr. In the most recent decade, mass contributions stabilized at 2.88 ± 0.09 mm/yr, while thermosteric trends remained steady at 3.07 ± 0.18 mm/yr, reflecting sustained ocean warming. Concurrently, halosteric contributions became increasingly negative, reaching −1.45 ± 0.06 mm/yr in 2013–2023 (Fig. 9c) consistent with increased salinity, which raises water density and reduces the height of the water column, thus lowering sea level. This intensification, as the GCLME transitions toward the Benguela system, underscores the growing dominance of mass-related SLR, compounded by thermal expansion and freshwater influxes, which are both projected to intensify under ongoing climate change[55,58].

The BCLME (Fig. 6c), stretching along the coasts of Angola, Namibia, and South Africa, is a wind-driven upwelling system and one of the world's four major eastern boundary current upwelling regions[59]. From 1993 to 2023, the region recorded SLA trend of 2.98 ± 0.05 mm/yr (Fig. 6c), slightly below the GMSL. This rise is dominated by manometric (mass) contributions (2.52 ± 0.05 mm/yr), accounting for 85% of the total increase. A significant portion of the mass-driven rise is attributed to gravitational redistribution from Antarctic ice melt, which disproportionately affects the South Atlantic, and to regional upwelling dynamics that modulate local sea level[55,57]. Steric contributions remain modest (0.34 ± 0.03 mm/yr, 15%) due to the upwelling of cooler, nutrient-rich waters that suppress thermosteric expansion[55]. Thermosteric expansion is measured at 0.46 ± 0.03 mm/yr, but this is further reduced by slight halosteric contraction (−0.12 ± 0.02 mm/yr), indicating a net reduction in sea level contribution, likely driven by increased salinity due to enhanced evaporation or reduced freshwater input[53]. This balance of forces reflects the region's sensitivity to both large-scale cryospheric changes (such as Antarctic meltwater) and local oceanographic processes (such as persistent upwelling)[55]. Decadal variability reveals a strong acceleration in SLA, rising from 2.13 ± 0.22 mm/yr in 1993–2002 (Figs. 9a) to 4.90 ± 0.17 mm/yr in 2013–2023 (Fig. 9c) more than doubling over the period, with a 2.3-fold increase. Early in the record, SLA was mainly driven by thermosteric expansion (2.65 ± 0.20 mm/yr) amid negligible or even negative manometric input (-0.23 ± 0.13 mm/yr). By the most recent decade, mass contributions surged 13-fold to 3.19 ± 0.10 mm/yr, reflecting intensified Antarctic meltwater input and the increasing dominance of mass-driven SLR in the region. Thermosteric trends also rose to 2.98 ± 0.16 mm/yr but were offset by strong halosteric contraction (−1.27 ± 0.09 mm/yr), driven by increased salinity, thereby reducing the net steric contribution to 15% of total SLR.

Indian Ocean LMEs. The ACLME, a warm western boundary current along South Africa's east coast, presents a SLA trend of 3.00 ± 0.09 mm/yr (Fig. 7a), ranking sixth among the seven African LMEs analyzed, slightly above the BCLME. This long-term SLA trend is primarily driven by manometric contributions, which account for 2.30 ± 0.05 mm/yr (~77%). These mass-driven changes are attributed to regional ocean mass redistribution, influenced by the intense eddy activity characteristic of the ACLME. Steric contributions account for the remaining ~23% (0.70 ± 0.07 mm/yr), but their influence is comparatively modest. Within the steric component, thermosteric expansion ranges from 0.45 ± 0.03 to 0.67 ± 0.08 mm/yr, reflecting upper-ocean warming. However, this warming effect is dampened by persistent eddy-induced cooling and vertical mixing, which reduce the net thermal expansion[60]. Halosteric effects are minimal to slightly negative, ranging from −0.10 ± 0.02 to 0.02 ± 0.02 mm/yr (Fig. 7a), indicating weak salinity-driven contributions that marginally oppose thermal expansion. These effects further limit the overall steric contribution to the SLA trend. The region's dynamic oceanography is characterized by strong decadal variability, driven by shifts in eddy activity, mass inflow, and upper-ocean heat content. During the period 1993–2002 (Fig. 9a), SLA exhibited a negative trend of −1.72 ± 0.65 mm/yr, driven primarily by strong cooling eddies and a large negative manometric contribution (−3.10 ± 0.20 mm/yr), while the thermosteric term was modestly positive (+1.45 ± 0.55 mm/yr) and the halosteric term slightly negative (−0.07 ± 0.06 mm/yr). These modest steric offsets were insufficient to counter the mass loss. This negative phase reflects reduced ocean mass input, linked to weakened current strength and shifts in regional atmospheric forcing, consistent with broader climate variability along the southeastern African coast.

In contrast, the period 2003–2012 saw a sharp rise in SLA, with trends reaching 2.81 ± 0.35 mm/yr (Fig. 9b). This increase was supported primarily by rising manometric contributions (2.81 ± 0.18 mm/yr), associated with intensified mass inflow into the region. This positive shift aligns with strengthened eddy activity and increased regional circulation, which enhanced ocean mass accumulation and contributed to upper-ocean warming despite persistent mixing. Between 2013 and 2023, SLA stabilized

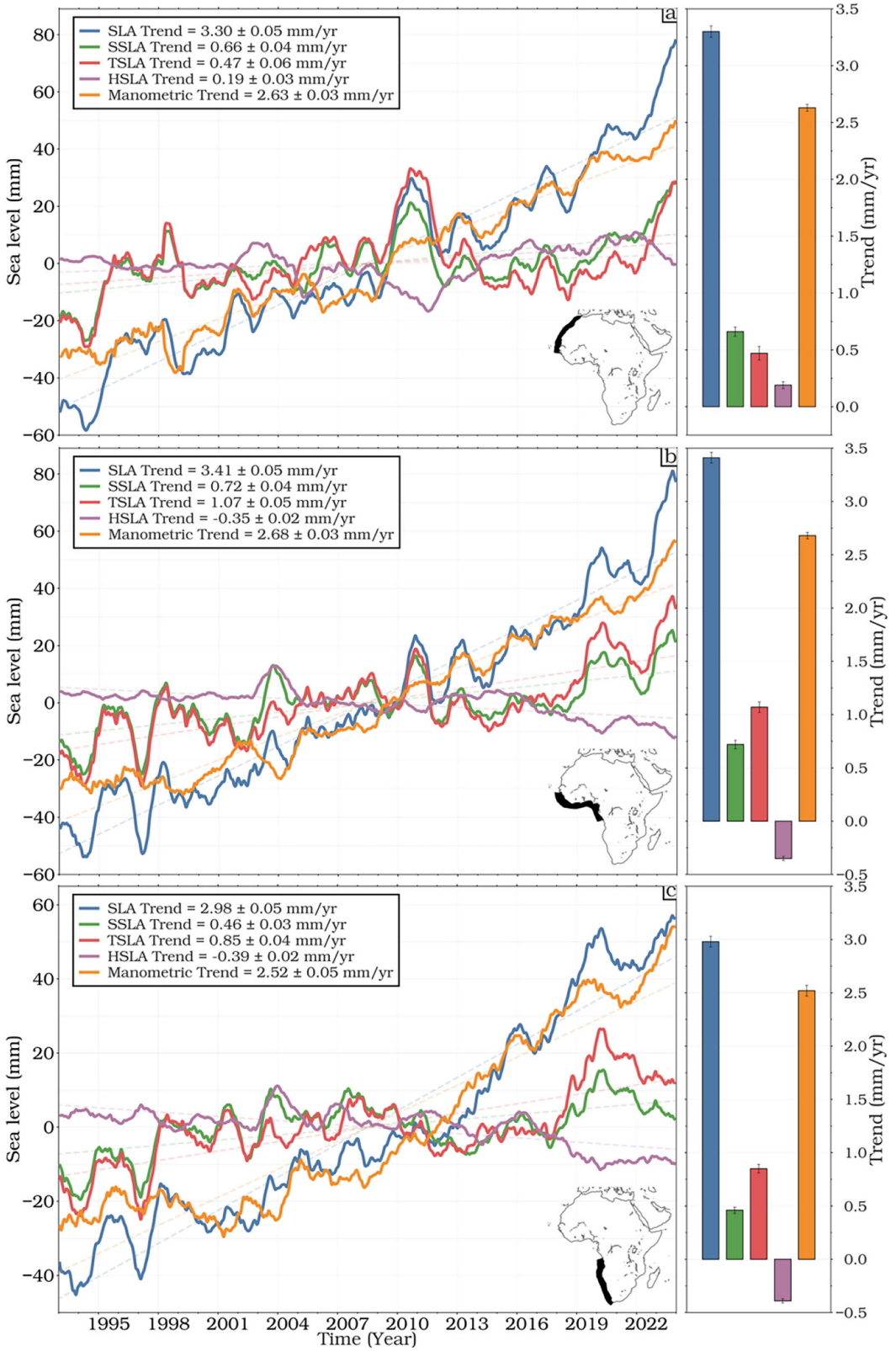

Fig. 6 | Regional sea level budget components for the Atlantic LMEs. Temporal evolution and linear trends of de-seasoned monthly anomalies for **a** the Canary Current LME (CCLME), **b** the Guinea Current LME (GCLME), and **c** the Benguela Current LME (BCLME) from 1993–2023. Contributions shown are total Sea-Level Anomaly (SLA; blue line), steric (SSLA; green line), thermosteric (TSLA; red line), halosteric (HSLA; purple line), and manometric (orange line). All time series are smoothed with a 13-month low-pass filter.

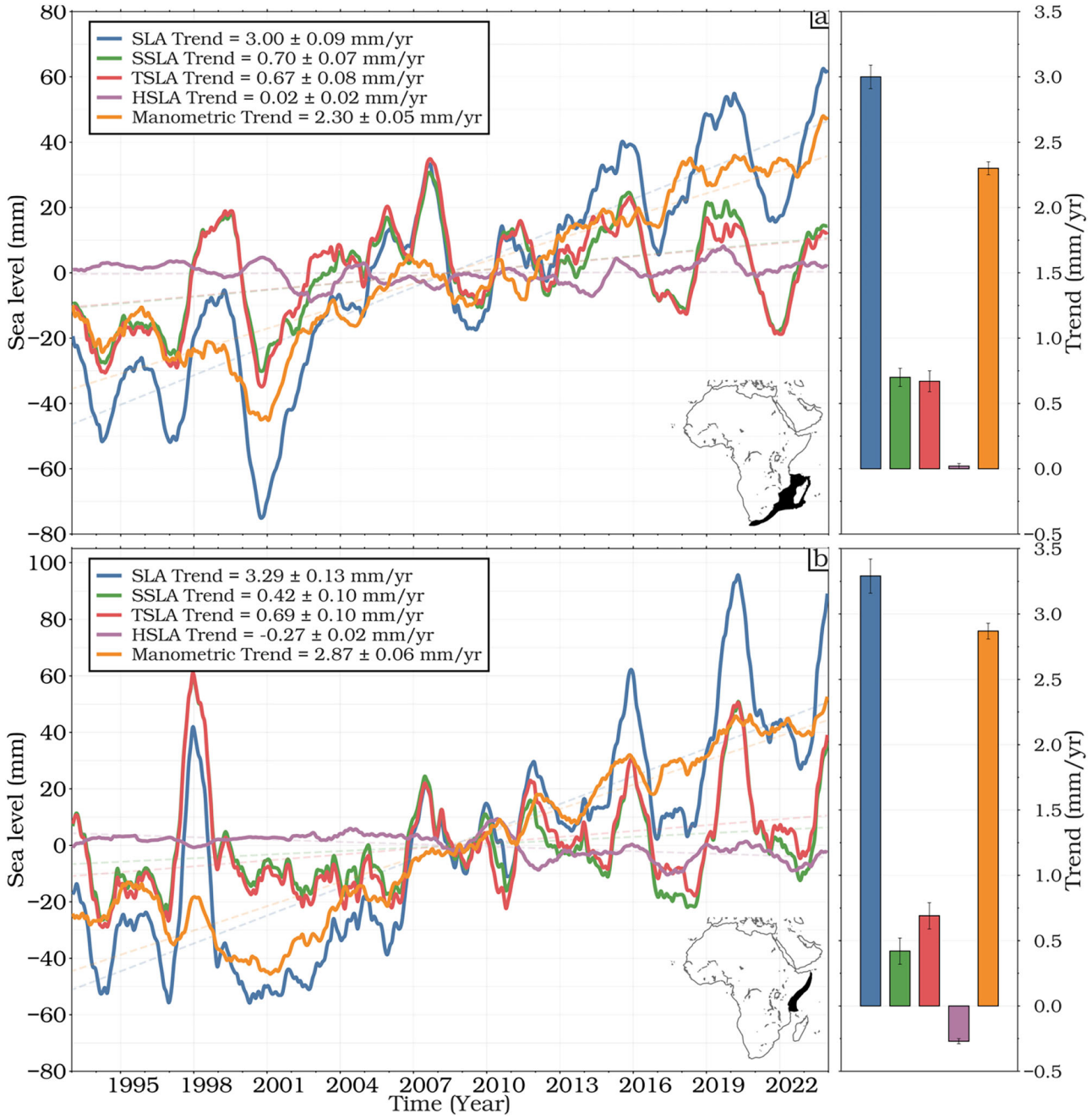

Fig. 7 | Regional sea level budget components for the Indian Ocean LMEs. Temporal evolution of sea level budget components for **a** the Agulhas Current LME (ACLME) and **b** the Somali Coastal Current LME (SCCLME) from 1993 to 2023. Contributions shown are total Sea-Level Anomaly (SLA; blue line), steric (SSLA; green line), thermosteric (TSLA; red line), halosteric (HSLA; purple line), and manometric (orange line). All time series are smoothed with a 13-month low-pass filter.

at 1.12 ± 0.39 mm/yr, with mass contributions (2.45 ± 0.13 mm/yr) continuing to dominate (Fig. 9c). However, thermosteric trends remained negative (−2.02 ± 0.32 mm/yr), suppressing steric input to just 23% of the total rise. This underscores the ACLME's sensitivity to dynamic ocean processes, where local steric effects are frequently modulated by turbulent mixing and eddy variability.

Along East Africa's Indian Ocean coast, the SCCLME unveils a SLA trend of 3.29 ± 0.13 mm/yr, ranking third among African LMEs (Fig. 7b). This trend is primarily driven by manometric contributions, which dominate the signal at 2.87 ± 0.06 mm/yr, accounting for 87% of the total rise. These mass-driven changes are largely attributed to global ice mass loss and monsoon-enhanced circulation, underscoring the critical role of ocean mass in shaping regional sea-level dynamics[61,62]. While smaller in magnitude, the steric contribution also plays a role in the SLA trend, with a net steric contribution of 0.42 ± 0.04 mm/yr. This is primarily driven by thermosteric expansion, which contributes 0.50 ± 0.04 mm/yr, reflecting modest ocean warming in the region. In contrast, halosteric effects are negligible, with a slight negative trend of –0.08 ± 0.02 mm/yr, indicating that increased salinity (density) slightly offsets the thermosteric expansion. This interplay between steric and manometric components highlights the dominance of mass-driven processes in the SCCLME, while steric contributions remain secondary. The sea-level budget also reveals pronounced decadal variability, reflecting the dynamic interplay of physical processes over time. During the period 1993–2002 (Fig. 9a), SLA trends were negative at –1.90 ± 0.88 mm/yr, driven by declines in both manometric (–2.97 ± 0.24 mm/yr) and thermosteric (1.01 ± 0.79 mm/yr) contributions. This period of reduced SLR

coincided with weak monsoonal forcing[63], which likely suppressed ocean circulation and upper-ocean heat content, reducing both mass and steric contributions. In contrast, the period 2003–2012 marked a sharp acceleration in SLA, with trends peaking at 5.92 ± 0.44 mm/yr (Fig. 9b). This dramatic increase is likely to be driven by strengthened monsoonal winds[64] and enhanced ocean warming, as reflected in significant gains in both manometric (3.93 ± 0.12 mm/yr) and thermosteric (2.28 ± 0.43 mm/yr) contributions. The intensified monsoonal forcing during this decade likely enhanced upper-ocean heat content and circulation, amplifying both steric and mass-driven SLR. The most recent decade, 2013–2023, shows a sustained SLA trend of 4.72 ± 0.67 mm/yr (Fig. 9c), slightly lower than the previous decade but still elevated. This trend remains primarily driven by manometric contributions (3.44 ± 0.15 mm/yr), which continue to dominate the sea-level budget with an 87% share.

However, the thermosteric contribution decreased to 1.50 ± 0.25 mm/yr, reflecting a slight reduction in ocean warming compared to the previous decade. Despite this decline, the dominance of mass-driven processes persists, underscoring the critical role of global ice mass loss and monsoonal dynamics in shaping regional sea-level trends. Looking ahead, the anticipated succession of El Niño and La Niña phases is expected to intensify interannual variability in the SCCLME. These climate oscillations are likely to modulate monsoonal wind patterns, upwelling strength, and upper-ocean heat content, potentially amplifying both thermosteric and manometric contributions to regional SLR.

Semi-Enclosed Basin LMEs. The REDLME exhibits the highest SLA trend among African LMEs, measured at 3.91 ± 0.13 mm/yr (Fig. 8a). This pronounced trend is primarily driven by the manometric contribution (2.06 ± 0.08 mm/yr), which accounts for 53% of the total rise, while thermosteric expansion (1.84 ± 0.09 mm/yr) accounts for 47%. The confined bathymetry and limited water exchange of the Red Sea enhance heat retention, amplifying upper-ocean warming and contributing significantly to the observed thermosteric trends. In contrast, halosteric effects (0.01 ± 0.02 mm/yr) are negligible, indicating minimal salinity-driven density changes and limited impact on steric sea level variations in this region. Together, the steric contribution totals 1.85 ± 0.09 mm/yr, underscoring the combined influence of temperature and salinity on SLR in this region. The decadal variability of SLA in the Red Sea LME highlights the dynamic interplay between regional temperature, salinity, and mass-driven processes. During the period 1993–2002 (Fig. 9a), SLA exhibited a strongly negative trend of −7.14 ± 0.51 mm/yr, driven by significant declines in both thermosteric (−4.27 ± 0.27 mm/yr) and manometric (−3.25 ± 0.37 mm/yr) contributions. This period of negative trends reflects regional cooling and reduced mass inputs, likely linked to weakened trade winds[65] and lower heat retention. In contrast, the period 2003–2012 (Fig. 9b) marked a dramatic reversal, with SLA peaking at 6.18 ± 0.59 mm/yr. This sharp increase was driven by thermosteric contributions (2.89 ± 0.60 mm/yr), reflecting intensified upper-ocean warming, and manometric contributions (2.66 ± 0.27 mm/yr), associated with wind-driven mass inflow. The warming trends during this decade highlight the Red Sea's sensitivity to regional and global climate forcing, as its confined geography amplifies heat accumulation and limits heat dissipation. By the period 2013–2023 (Fig. 9c), SLA trends stabilized at 3.55 ± 0.43 mm/yr, with thermosteric expansion (3.23 ± 0.40 mm/yr) emerging as the dominant driver. During this time, manometric contributions dropped to 0.01 ± 0.42 mm/yr, indicating a reduced influence of mass-driven processes, such as wind-driven inflow or regional mass redistribution. The sustained thermosteric trends, however, underscore the persistent warming of the Red Sea's water column, which continues to drive SLR in the absence of significant salinity-driven or mass-driven changes. The observed SLA trends in the Red Sea LME are closely tied to the region's unique oceanographic conditions, limited water exchange, and sensitivity to atmospheric forcing. The strong connection between SLA and temperature trends in the water column highlights the critical role of heat retention in driving thermosteric expansion. While salinity trends remain minimal, their slight variability contributes to the overall steric balance. The decadal shifts in SLA further emphasize the influence of regional climate variability, including trade wind patterns and heat fluxes, on the Red Sea's dynamic sea-level budget.

The MEDLME, the northernmost of the African LMEs, exhibits the lowest SLA trend among them, with an average rise of 2.70 ± 0.06 mm/yr from 1993 to 2023 (Fig. 8b), representing the lowest trends across African LMEs during the analysis period (see Table 1). This reduced SLA trend is primarily attributed to strong negative halosteric effects (-1.03 ± 0.04 mm/yr) caused by reduced Nile River discharge and high evaporation rates, which increase salinity and density, thereby counteracting thermosteric expansion. In contrast, other African LMEs, such as the Red Sea (3.91 ± 0.13 mm/yr) and the Guinea Current (3.41 ± 0.05 mm/yr), exhibit higher SLA trends due to the dominance of mass-driven contributions and weaker salinity-driven suppression. The manometric contribution in the Mediterranean, which includes the effects of oceanic mass change and redistribution and changes in bottom pressure caused by ocean currents[55], accounts for 1.78 ± 0.07 mm/yr, representing 66% of the total SLA trend. Groundwater extraction and tectonic activity may also contribute to the residual trend. Meanwhile, thermosteric expansion contributes 1.95 ± 0.04 mm/yr, but this is significantly offset by salinity-driven contraction, resulting in a net steric contribution of 0.92 ± 0.05 mm/yr (34%). Decadal trends reveal substantial variability in SLAs, reflecting the dynamic interplay of physical oceanographic processes. Between 1993 and 2002 (Fig. 9a), SLA rose at 3.94 ± 0.32 mm/yr, primarily driven by strong thermosteric expansion (4.50 ± 0.10 mm/yr) associated with upper-ocean warming[66,67], while manometric contributions were minimal (−0.35 ± 0.26 mm/yr), underscoring the dominance of temperature-induced changes during this period. From 2003 to 2012 (Fig. 9b), SLA accelerated to 5.32 ± 0.42 mm/yr, coinciding with a significant rise in manometric contributions (3.18 ± 0.42 mm/yr) linked to ocean mass redistribution, bottom pressure changes, and wind-driven circulation[68,69]. Meanwhile, steric contributions weakened to 2.13 ± 0.22 mm/yr as emerging negative halosteric trends (−1.88 ± 0.15 mm/yr) began to offset thermosteric expansion. In the Mediterranean Sea, SLA deceleration was primarily driven by intensified salinity effects: negative halosteric trends, indicating increased salinity, reduced SLA by 0.82 mm/yr, thereby diminishing both thermosteric and manometric contributions[66,70].

This highlights the Mediterranean as a key region for understanding salinity-driven suppression of SLR. During the most recent decade (2013–2023, Fig. 9c), SLA growth slowed to 2.71 ± 0.30 mm/yr, representing a 31% decrease from the 2003–2012 peak and 1.24 mm/yr below the early period's rate. This decline reflects a shift in ocean dynamics, with steric contributions accounting for only 34% of the total SLA during this period. Negative steric trends (−0.93 ± 0.20 mm/yr), dominated by halosteric suppression (−2.86 ± 0.07 mm/yr), played a key role in this slowdown. While unusually large for a halosteric contribution, this value is supported by the data and may reflect intense regional salinification. Although manometric contributions increased to 3.64 ± 0.34 mm/yr, their effect was largely offset by the persistent influence of salinity. The Mediterranean's low SLA trend is justified by its unique salinity-driven suppression of SLR, which distinguishes it from other African LMEs where mass-driven SLR typically dominates. For example, the Red Sea exhibits the highest SLA trend (3.91 ± 0.13 mm/yr, Fig. 8a) due to strong manometric contributions from ice melt and water mass redistribution, while the Guinea Current (3.41 ± 0.05 mm/yr, Fig. 6b) and Canary Current (3.30 ± 0.05 mm/yr, Fig. 6a) are similarly influenced by mass-driven processes. In contrast, the Mediterranean's sensitivity to hydrological changes, including reduced riverine input, high evaporation, and regional climate variability, results in a distinct response characterized by salinity-driven contraction. The inclusion of manometric contributions, which encompass oceanic mass redistribution, bottom pressure changes, and local vertical land movements, helps disentangle the competing drivers of SLA in this region and reinforces the central role of salinity changes in modulating sea-level trends.

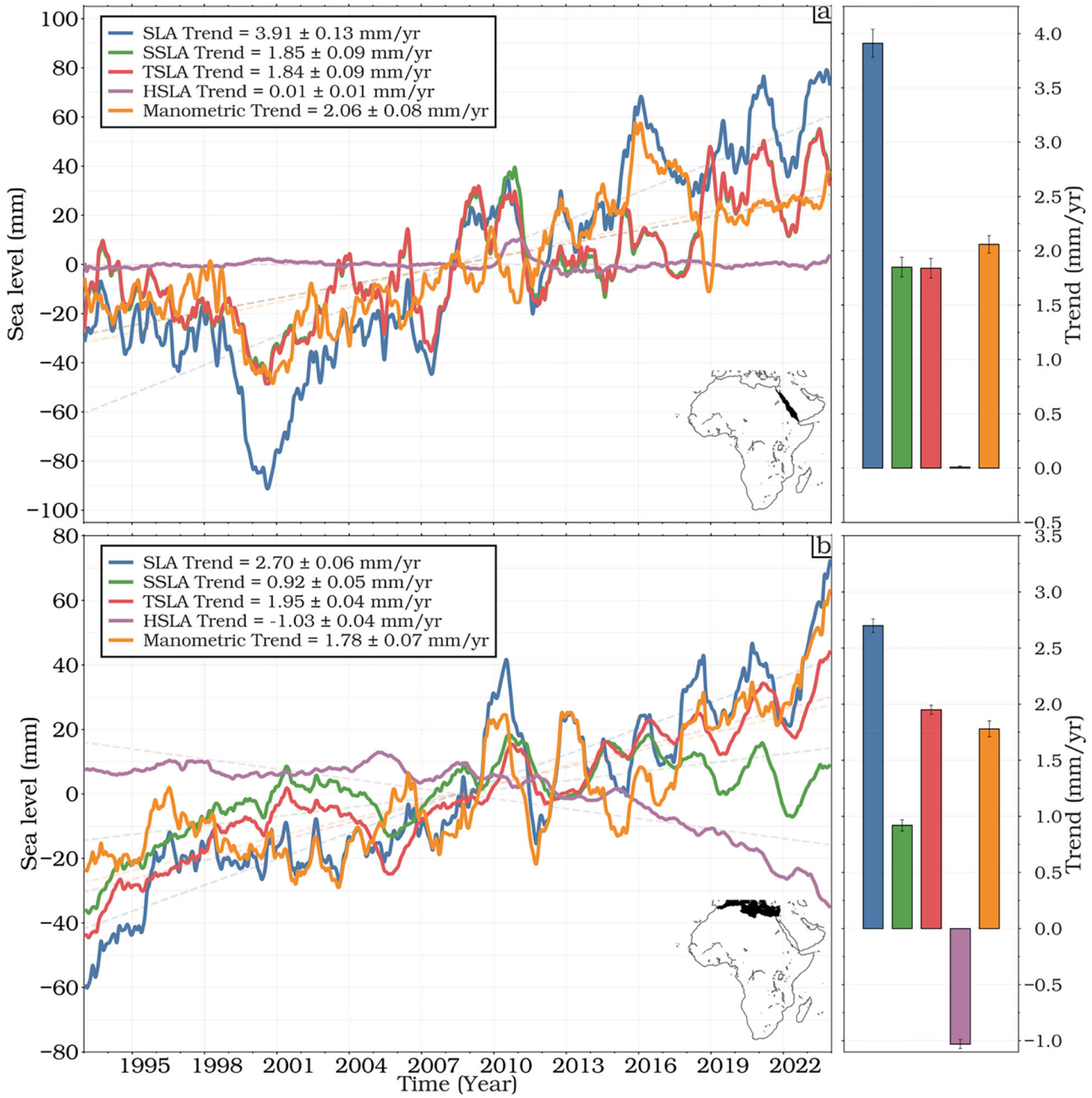

Fig. 8 | Regional sea level budget components for the Red Sea and Mediterranean Sea LMEs. Temporal evolution of sea level budget components for **a** the Red Sea LME (REDLME) and **b** the Mediterranean Sea LME (MEDLME) from 1993 to 2023. Contributions shown are total Sea-Level Anomaly (SLA; blue line), steric (SSLA; green line), thermosteric (TSLA; red line), halosteric (HSLA; purple line), and manometric (orange line). All time series are smoothed with a 13-month low-pass filter.

Ocean-atmosphere interactions and sea level variability in African LMEs

Climate modes drive large-scale patterns of sea level variability across ocean basins, as noted by Han et al.[71]. In the context of Africa's seven LMEs, the influence of these modes varies between the open ocean and coastal regions, particularly along the EBUS of the Canary and Benguela Currents. SLAs along these eastern boundaries are predominantly influenced by remote and local wind forcing, which propagates through equatorial and coastal waveguides[14,34]. In contrast, SLAs in the interior of these LMEs are driven by open-ocean forcing that propagates westward from the eastern boundaries. Consequently, coastal sea level variability in African LMEs is expected to correlate strongly with climate modes that are prominent in the tropics and with atmospheric centers of action that modulate longshore winds and sea level pressure.

The regression of SLA with respect to climate indices is shown in Fig. 10 (the corresponding correlation map is provided in Supplementary Fig. 3). Starting with the Atlantic Niño (ATL3) in Fig. 10a, a strong positive regression emerges along both Atlantic and equatorial domains, especially along the Gulf of Guinea and extending westward. This pattern reflects the role of ATL3 in modulating SLA through SST anomalies, which drive thermal expansion and mass redistribution in the ocean. The influence of ATL3 is most pronounced in the GCLME, BCLME, and SCCLME, but it diminishes both northward toward the Canary and southward toward the Benguela Current, indicating a more localized impact of ATL3 on SLA variability, largely confined to the tropics. Transitioning to the Tropical North Atlantic (TNA) index in Fig. 10b, the regression map reveals pronounced positive anomalies along the northern tropical Atlantic, with significant effects extending into the Canary Current LME and the

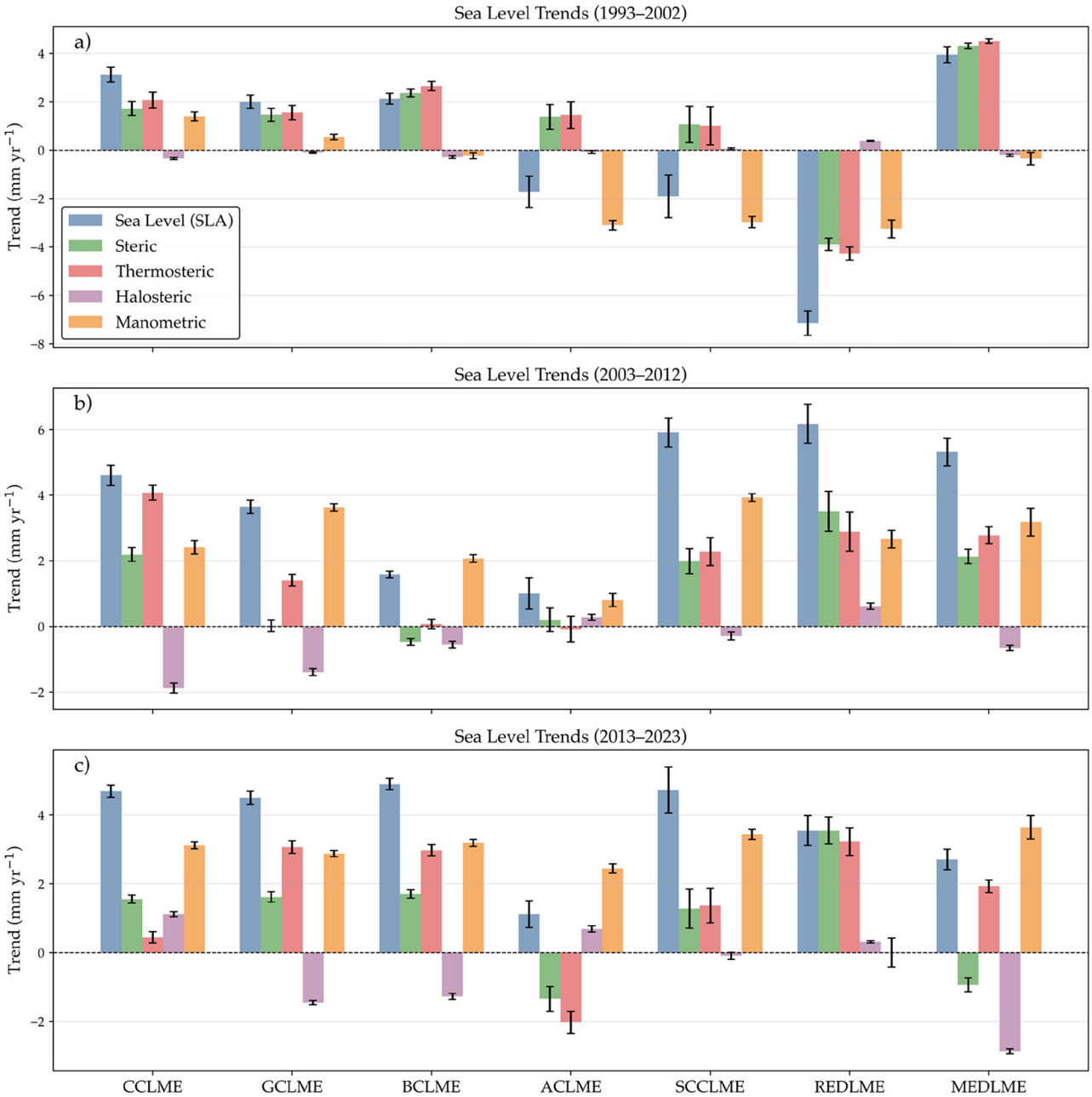

Fig. 9 | Decadal sea level budgets across African LMEs. Histograms of decadal sea-level budgets for **a** 1993–2002, **b** 2003–2012, and **c** 2013–2023 across Africa's LMEs.

Mediterranean Sea. This underscores the importance of SST anomalies in the Tropical North Atlantic, which drive SLA variability through atmospheric teleconnections and oceanic processes such as wind-driven circulation and heat fluxes. However, the influence of TNA fades in the southern LMEs, including GCLME, BCLME, ACLMEs, and SCCLME, highlighting the regional specificity of this index and its primary relevance to the northern Atlantic margin with no impact on the REDLME. The Tropical Atlantic SST Gradient Index (TASI), shown in Fig. 10c, captures the meridional SST gradient in the Atlantic and exhibits a dipolar pattern, with positive regression coefficients in the northern Atlantic while not significant as the TNA and negative coefficients in the southern Atlantic. This spatial structure emphasizes the role of TASI in modulating SLA through changes in the interhemispheric SST gradient, which in turn affects wind patterns and ocean circulation. The Canary and Benguela Current LMEs are particularly sensitive to TASI, as these regions are directly influenced by shifts in the Atlantic dipole mode, while the Mediterranean LME and other LMEs remain less affected. Moving eastward, Fig. 10d presents the regression of SLA on the Indian Ocean Dipole (DMI). Here, strong positive coefficients dominate the western Indian Ocean, especially along the Somali Current LME and extending into the Agulhas Current LME. This dipolar pattern reflects the DMI's capacity to drive SLA variability through SST changes and associated atmospheric circulation, with the Somali Current LME being especially responsive to the western Indian Ocean's warming and mass redistribution. The Atlantic LMEs, by contrast, show minimal response to DMI, underscoring the basin-specific nature of this influence. The Western Tropical Indian Ocean (WTIO) index, depicted in Fig. 10e, further reinforces the dominance of the western Indian Ocean, with a pronounced positive regression along the Somali and Agulhas Current LMEs. The influence of WTIO even extends into the Red Sea Current outlets through the Gulf of Aden, highlighting the significant role of SST anomalies in this region in driving SLA variability through thermal expansion and changes in ocean circulation. However, the impact of WTIO diminishes toward the

Table 1 | SLA and contributing trends from 1993 to 2023 (mm/yr)

Rank	Region/LME	SLA	Steric	Thermosteric	Halosteric	Manometric	Primary driver
1	REDLME	3.91 ± 0.13	1.85 ± 0.09	1.84 ± 0.09	0.01 ± 0.01	2.06 ± 0.08	Manometric
2	GCLME	3.41 ± 0.05	0.72 ± 0.04	1.07 ± 0.05	−0.35 ± 0.02	2.68 ± 0.03	Manometric
3	CCLME	3.30 ± 0.05	0.66 ± 0.04	0.47 ± 0.06	0.19 ± 0.03	2.63 ± 0.03	Manometric
4	SCCLME	3.29 ± 0.13	0.42 ± 0.10	0.69 ± 0.10	-0.27 ± 0.02	2.87 ± 0.06	Manometric
5	BCLME	2.98 ± 0.05	0.46 ± 0.03	0.85 ± 0.04	−0.39 ± 0.02	2.52 ± 0.05	Manometric
6	ACLME	3.00 ± 0.09	0.70 ± 0.07	0.67 ± 0.08	0.02 ± 0.02	2.30 ± 0.05	Manometric
7	MEDLME	2.70 ± 0.06	0.92 ± 0.05	1.95 ± 0.04	−1.03 ± 0.04	1.78 ± 0.07	Thermosteric

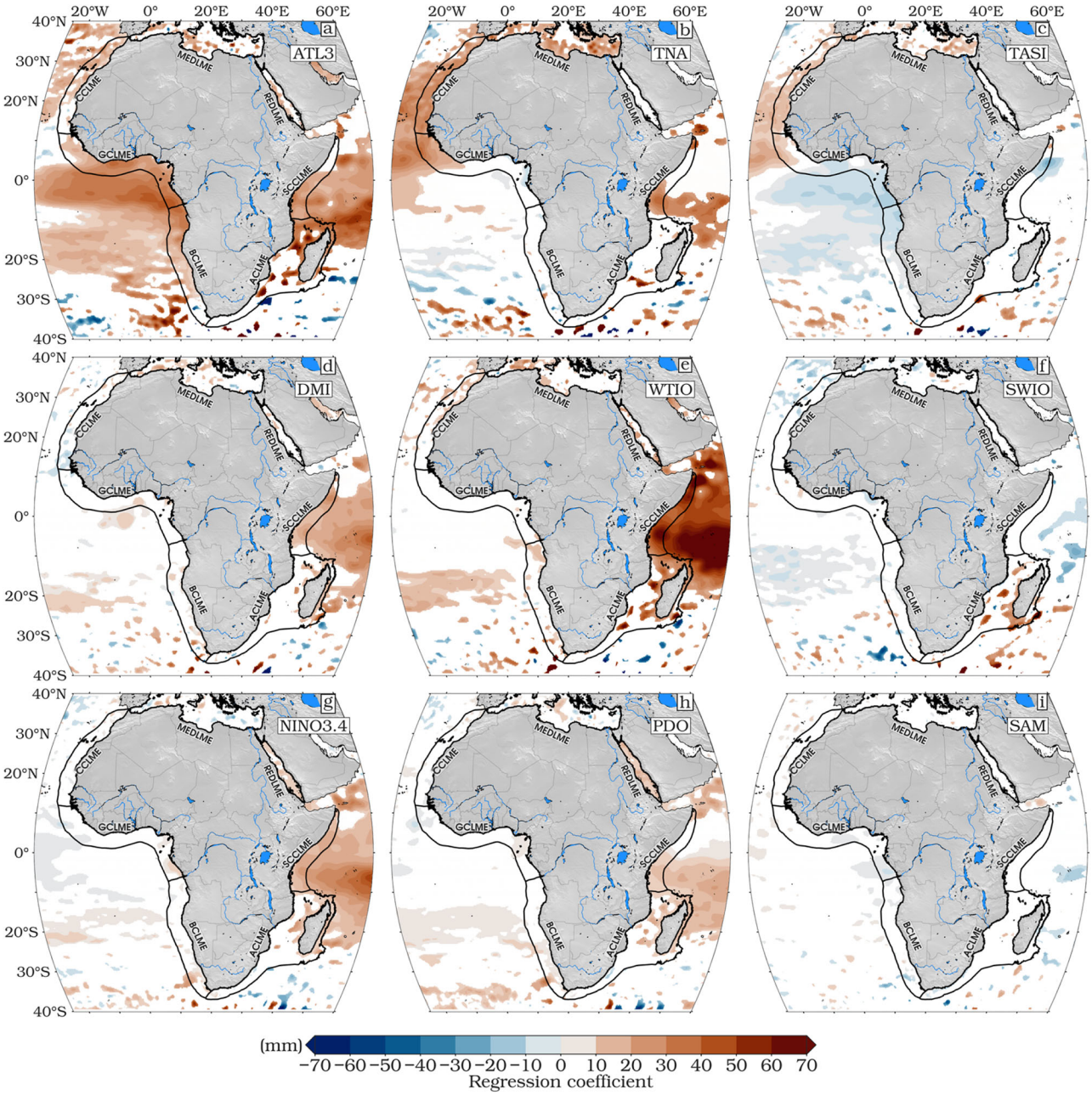

Fig. 10 | Relationship between African sea level and major climate indices. Linear regression coefficients (mm) of sea level over Africa and its LMEs with respect to **a** ATL3, **b** TNA, **c** TASI, **d** DMI, **e** WTIO, **f** SWIO, **g** NINO 3.4, **h** PDO, and **i** SAM. White areas (white dots) indicate regions where regression coefficients are not statistically significant at the 95% confidence level.

northern LMEs, such as the Mediterranean and Canary Currents, again reflecting the regional specificity of this index. A similar spatial pattern is observed for the Southwest Indian Ocean (SWIO) index in Fig. 10f, where sporadic positive regression coefficients are concentrated in the southwestern Indian Ocean. The Agulhas Current LME is particularly affected by SWIO, as this region is directly influenced by warming and mass redistribution in the southwestern Indian Ocean, mostly along the Madagascar coastal domain. In contrast, the Atlantic LMEs remain largely unaffected by SWIO, further emphasizing the spatial selectivity of Indian Ocean climate drivers. The influence of the central Pacific is captured by the Niño3.4 index in Fig. 10g, which shows a widespread impact across both the Indian Ocean and less impact on the Atlantic Ocean. Positive regression coefficients are evident in the western Indian Ocean close to the DMI patterns. This pattern reflects the teleconnections between the Pacific and other ocean basins, where changes in atmospheric circulation and oceanic processes driven by Pacific SST variability propagate their effects. The Somali and Red Sea Current LMEs are particularly sensitive to Niño3.4, while the Mediterranean and Agulhas LMEs remain less affected, indicating the reach but also the limits of Pacific influence. The Pacific Decadal Oscillation (PDO) (Fig. 10h) exhibits a notable large-scale influence on sea level variability, primarily across the Indian Ocean sector of the African LMEs. Positive regression coefficients are particularly evident in the Somali, Red Sea, and Agulhas Current LMEs, indicating that positive phases of the PDO typically associated with cooler SSTs in the western Pacific and warmer conditions in the eastern Pacific coincide with SLR in these regions. This response reflects enhanced Indian Ocean warming during positive PDO phases, which promotes upper-ocean thermal expansion and SLAs[71,72]. The Agulhas Current LME's sensitivity may be linked to PDO-induced modulation of the Indian Ocean Walker circulation and subtropical gyre dynamics, influencing the transport and convergence of water masses along southeast Africa. In contrast, Atlantic LMEs, including the Guinea Current and Canary Current systems, show limited correlation with PDO, likely due to weaker atmospheric teleconnections between the Pacific and Atlantic basins in decadal timescales[73]. The Southern Annular Mode (SAM) (Fig. 10i), which reflects the north–south displacement of the westerly wind belt encircling Antarctica, shows no statistically significant impact on sea level trends across any African LMEs. This limited influence is consistent with previous findings that SAM-driven sea level variability is largely confined to southern extratropical latitudes, particularly the Southern Ocean and the high-latitude South Atlantic and Indian sectors[74]. As a result, the absence of significant regression patterns in African LMEs suggests that SAM's dynamical effects on wind stress, Ekman transport, and associated mass redistribution do not strongly project onto the sea level variability of equatorial or subtropical African coastal systems.

Summary and discussion

Accelerating global warming has intensified SLR along Africa's coastal regions, creating unprecedented challenges for climate adaptation. Recent findings by Forster et al.[75] reveal that the decade from 2014 to 2023 experienced an average global warming of 1.19 °C above pre-industrial levels, primarily due to anthropogenic emissions. In 2023 alone, the temperature anomaly reached 1.31 °C, further amplified by natural variability[76]. This unprecedented warming rate of 0.26 °C per decade stems from persistently high greenhouse gas emissions (~53 ± 5.4 Gt CO_2e annually) and a diminishing aerosol cooling effect[75]. These global climate trends are directly reflected in the SLAs across Africa's seven LMEs, with 2023 marking a critical turning point for the continent.

Between 1993 and 2023, mean sea levels across African LMEs rose by approximately 10.25 cm, equivalent to a linear trend of 3.31 ± 0.04 mm/yr. However, this average masks substantial spatial variability driven by complex interactions between thermosteric (temperature-induced), halosteric (salinity-induced), and manometric (mass-related) contributions. As shown in Table 1, all seven LMEs exhibited positive full-period trends (~2.70–3.91 mm/yr), yet the dominant physical drivers and their decadal evolution differ sharply across regions. In some basins (REDLME, BCLME), thermosteric expansion is the main contributor, while in others (MEDLME, GCLME, SCCLME), halosteric changes offset or modulate the warming signal, and since the early 2000s, manometric loading has surged to 2–3.6 mm/yr in most regions.

The pace of change has accelerated dramatically over the past two decades, with global SLR rates reaching 3.80 ± 0.8 mm/yr from 2002 to 2023, exceeding the 3.52 ± 0.47 mm/yr observed over the full altimetric record (1993–2023). This recent acceleration is increasingly mass-driven in several key LMEs, such as the GCLME, where ocean mass addition has remained strong (~2.9–3.6 mm/yr since 2003), and the REDLME, where the last decade's rise has been almost entirely steric and dominated by exceptional thermosteric gains (+3.23 mm/yr), with minimal halosteric offset due to stable salinity. These rising baselines elevate flood risks and erosion potential in low-lying deltas and urban zones, increasing the frequency of nuisance flooding and threatening coastal stability. The resulting physical impacts directly undermine SDG 14 (Life Below Water) by intensifying stress on marine habitats such as coral reefs, mangroves, and salt marshes, and SDG 11 (Sustainable Cities and Communities) by reducing the resilience of coastal settlements, infrastructure, and livelihoods against climate-driven sea-level hazards. At the heart of these trends lies Earth's persistent energy imbalance (~0.9 W m^{-2}), with oceans absorbing over 90% of excess heat driving both thermal expansion and accelerated land ice melt[75,77]. Recent research reveals that global ocean heat content has nearly doubled since 2010, with most heat accumulating in the upper 2000 m[78]. This pattern reflects the intensification of anthropogenic warming and its profound impact on ocean dynamics[79]. Consequently, the effects of these global processes manifest unevenly along Africa's margins, creating distinct regional patterns of sea-level change.

Nowhere is the temporal variability more striking than in several of Africa's LMEs, particularly the REDLME in the east and the GCLME in the west, the two highest-SLR LMEs on the continent, at 3.91 ± 0.13 mm/yr and 3.41 ± 0.05 mm/yr, respectively. Looking beyond these full-period averages, the REDLME shows one of the most abrupt decadal reversals anywhere along Africa's coasts—shifting from a sharp SLA fall in 1993–2002 (~ − 7.14 mm/yr) to a rapid rise in 2003–2012 (~ + 6.18 mm/yr), and then to a still-positive, steric-dominated phase in 2013–2023 (+3.55 mm/yr, almost all thermosteric at +3.23 mm/yr). Similar stark regime shifts occurred in the ACLME (from −1.72 mm/yr to +1.01 mm/yr) and SCCLME (from −1.90 mm/yr to +5.92 mm/yr), highlighting coherent East African LME responses likely modulated by regional climate-ocean drivers such as the IOD and ENSO. In the REDLME, a strong and sustained thermosteric rise over the past two decades, largely unmitigated by salinity changes, aligns with its very high global coral-bleaching importance, since ongoing thermal ocean warming has increased the frequency and severity of marine heatwaves[80]—the proximate causes of coral bleaching in this region. In the GCLME, a mass-dominated rise has combined with halosteric contraction (salinification) to overwhelm vertical accretion in mangrove and salt marsh systems, raise hydroperiods in subsiding deltas, and exacerbate salinity stress, particularly in the Niger Delta, Lagos coast, and the barrier-lagoon complexes from Benin to Côte d'Ivoire. Negative halosteric trends here (−1.45 mm/yr in 2013–2023) imply increasing density and reduced stratification at depth, which can facilitate saline intrusion upriver during dry periods, stressing mangroves and estuarine marshes. Both regions are largely driven by upper-ocean warming[7] process. In contrast, the MEDLME shows a more moderate increase of 2.70 ± 0.06 mm/yr, primarily linked to halosteric changes from high evaporation and limited freshwater input[69], with recent strong salinification (−2.86 mm/yr halosteric) amplifying density gradients that inhibit vertical mixing, potentially reducing nutrient delivery to coastal marsh lagoons. Notably, mass redistribution from ice sheet melt now accounts for over 80% of total sea-level anomaly across Africa, with Greenland and Antarctica alone contributing about 2.0 mm/yr to the global mean[75]. According to Nicholls et al.[81] high subsidence rates are widespread and not confined to a few well-known locations. Multiple African coastal cities and deltaic regions, including Alexandria and Port Said on the Nile Delta; Abidjan, Cotonou, Lagos, and Douala along the Gulf of

Guinea; and Mombasa and Maputo in East Africa, experience local land subsidence from groundwater extraction, sediment compaction, and infrastructure loading that adds several millimeters per year to climate-driven SLR. In many of these locations, relative SLR now exceeds6–18 mm/yr[58], substantially raising flood frequency and heightening exposure for millions of residents.

The recent acceleration in SLR has been particularly pronounced across African oceanic regions, surging from 0.96 ± 0.26 mm/yr (1993–2002) to 4.34 ± 0.18 mm/yr (2013–2023), outpacing the global acceleration rate. For the ACLME, the negative SLA phase of 1993–2002 (−1.72 mm/yr) was driven primarily by a large negative manometric term (−3.10 mm/yr) despite a modestly positive thermosteric contribution, before rebounding to positive, mass-dominated rises after 2003. SCCLME followed a similar pattern, emphasizing the east-African coherency of these regime shifts. In several LMEs, including the GCLME, the shift from mixed steric–mass contributions in the 1990s to a clear mass-dominated signal after 2003 marks a structural change in the hazard baseline—one that is now decoupled from interdecadal thermosteric variability. This trend reflects a persistent global energy imbalance of approximately 0.9 W/m², with thermosteric expansion now contributing about 1.4 mm/yr to SLR[75,82]. The year 2023 proved particularly significant, with sea levels rising by 1.97 cm from 2022 to 2023, marking the second highest annual increase on record. The ACLME was especially affected, as intensified mesoscale activity and El Niño-related SST anomalies (+0.8 °C) generated regional sea-level hotspots[7,83]. These anomalies far exceeded the global average annual rise of 0.59 cm, posing acute risks to Africa's low-lying coastal zones. Understanding the mechanisms driving these changes reveals the complexity of regional sea-level variability. These below-average trends align with regions of pronounced mesoscale eddy activity and complex current dynamics, particularly in the Mozambique Channel and southern Agulhas and Benguela systems[84,85], where frequent eddy formation and southward migration influence sea-level variability through lateral heat redistribution and kinetic energy dissipation. Steric contributions varied significantly by region, with thermosteric and halosteric effects together accounting for 40–50% of observed sea-level changes, aligning with global patterns[86]. In the REDLME, thermosteric expansion in 2013–2023 alone reached +3.23 mm/yr, a physical signal closely tied to elevated bleaching risk in one of the planet's most heat-tolerant coral provinces. In the GCLME, halosteric contraction has been consistently negative since 2003, possibly intensifying salinity intrusion in estuaries and compounding flood hazards from manometric loading. In 2023, thermosteric expansion in the REDLME reached 2.5 mm/yr, while marine heatwaves affected over 40% of the sea surface[79,87]. Halosteric effects were more pronounced in the GCLME and SCCLME, where enhanced rainfall from an intensified WAM caused SLA spikes of up to 8 cm, particularly near major river mouths like the Congo[14,34]. However, limited salinity data, especially in non-EBUS regions, constrains accurate quantification of halosteric trends, representing a critical observational gap. Manometric processes dominate in deltaic and subsiding areas such as the GCLME and CCLME, where ice melt and groundwater depletion have driven relative SLR to 18 mm/yr in places like Douala[18] and Lagos[20]. Furthermore, large-scale climate oscillations significantly modulate these regional dynamics, adding another layer of complexity to sea-level variability.

The 2023 El Niño, marked by strong Niño 3.4 SST anomalies, elevated sea levels in the SCCLME and triggered extreme rainfall that led to SLAs of up to 15 cm in the GCLME[14]. The Atlantic Niño intensified thermosteric rise in the GCLME and BCLME, with regression coefficients of 23.99 mm and 17.74 mm, respectively. Meanwhile, the Indian Ocean Dipole (DMI) played a key role in SLA variability in the ACLME and SCCLME, with positive phases increasing Congo River discharge by 20% and resulting in halosteric anomalies of up to 3 cm[88]. These climate-driven variations interact with the underlying trend of accelerating SLR to create compound hazards along African coastlines.

The intersection of SLR and extreme weather events creates increasingly dangerous compound hazards that threaten coastal communities across Africa. Rising temperatures amplify the frequency and intensity of heatwaves, droughts, and heavy rainfall, threatening public health, food security, infrastructure, and labor productivity[77]. In 2023, El Niño-driven rains caused severe flooding in Ghana and southern Nigeria, regions already experiencing SLR of nearly 4 mm/yr[89]. Simultaneously, devastating floods in the Horn of Africa, following the worst drought in four decades, displaced hundreds of thousands and destroyed critical infrastructure[90]. Cyclone Freddy and Storm Daniel, which affected over 4 million people across Mozambique, Malawi, and Libya, were amplified by a 7 cm sea-level anomaly linked to Atlantic Meridional Overturning Circulation (AMOC) variability[7,36]. Such compound events increasingly exceed adaptation capacity, particularly among vulnerable populations where maternal and reproductive health face heightened risks[55,77].

These physical changes translate into profound socioeconomic consequences across the continent. More than 250 million people living in African coastal zones face escalating risks of chronic flooding, infrastructure collapse, and saltwater intrusion, with vulnerability particularly acute in megacities like Lagos, Alexandria, and Dar es Salaam[91]. In Lagos alone, subsidence may double flood frequency by 2050, threatening over 12 million residents[15]. Projections indicate that up to 117 million Africans could be affected by a 0.3-m SLR by 2030[92]. This heightened vulnerability is compounded by rapid urbanization and inadequate coastal planning in many African cities, creating a cascade of interconnected risks.

Ecological impacts are equally alarming across Africa's marine ecosystems. In EBUS, like the Canary and Benguela Currents, warming reduces nutrient upwelling, undermining fishery productivity vital to food security[25,93]. In the REDLME and SCCLME, thermosteric warming accelerates mangrove dieback and coral bleaching, weakening natural coastal defences that protect communities from storm surges and erosion[94]. For island nations like Seychelles and Cape Verde, rising seas and intensifying storm surges threaten not only livelihoods and marine economies but also cultural heritage and national identity[28,69]. These ecological changes create feedback loops that further amplify human vulnerability, as degraded ecosystems provide less protection and fewer resources for coastal communities.

The climate justice implications of these findings cannot be overstated. Africa's negligible 4% contribution to global CO_2 emissions stands in stark contrast to the continent's disproportionate suffering from climate consequences[77]. This disparity highlights the urgent need for international climate finance and technology transfer to support African adaptation efforts. Moreover, the accelerating pace of change, with SLR rates increasing from 0.96 mm/yr in the 1990s to over 4.3 mm/yr in recent years, suggests that current adaptation strategies may be insufficient for the challenges ahead.

This comprehensive analysis reveals that SLR along Africa's coastlines represents one of the most pressing climate challenges of our time. The strong spatial signature of manometric changes underscores the vulnerability of African coastal LMEs to global mass fluxes, which heighten risks of coastal flooding and erosion. The convergence of accelerating physical changes, intensifying extreme events, and growing coastal populations creates a perfect storm of vulnerability that demands immediate and sustained action. The scientific evidence presented here underscores the critical need for integrated coastal management strategies that address both the physical drivers of sea-level change and the socioeconomic vulnerabilities they exacerbate. As Africa continues to experience the frontline impacts of global climate change, the international community must recognize that supporting African adaptation efforts is not only a moral imperative but also essential for global climate stability and security. The time for incremental responses has passed; the scale and urgency of the challenge require transformative action that matches the magnitude of the threat facing Africa's coastal regions.

Data and methodology

This study investigates the interannual variability and long-term trends in sea level within the Africa LMEs, focusing on steric (thermosteric and

halosteric), manometric, and atmospheric contributions. A combination of satellite, in situ, and reanalysis products was employed, as outlined below.

Satellite altimetry and climate indices

SLA were obtained from the Copernicus Marine and Environment Monitoring Service (CMEMS; DOI: 10.48670/moi-00148, accessed April 2025). The dataset, gridded at 0.25° × 0.25°, spans the period 1993–2023 and integrates observations from multiple satellite altimetry missions (Jason series, Sentinel-3A, HY-2A, Saral/AltiKa, CryoSat-2, TOPEX/Poseidon, ENVISAT, GFO, and ERS1/2). Standard corrections for instrumental biases, tidal effects, and dynamic atmospheric contributions (DAC) were applied. Specifically, DAC version 4.0, which includes wind effects and the inverted barometer (IB) correction, was used to isolate atmospheric influences on sea level variability[95]. Note that the SLA dataset had already been atmospherically corrected using this DAC product (AVISO; https://tds.aviso.altimetry.fr, accessed April 2025) and also was adjusted to account for drift in the TOPEX-A altimeter[96] and the Jason-3 radiometer, which influences the wet troposphere correction. To correct for GIA the viscoelastic response of the Earth to deglaciation and associated ocean basin redistribution, geoid height changes rates from the ICE6G-D model[97] were resampled to match the spatial resolution of the altimetry data.

Monthly time series of relevant climate indices (Supplementary Fig. 4) were used to examine the influence of large-scale climate variability on regional sea level.

These include:

Niño 3.4 Index. Represents central equatorial Pacific variability and is calculated as the area-averaged sea surface temperature (SST) anomaly over 170°W–120°W and 5°S–5°N. Positive anomalies are associated with El Niño events, typically peaking during boreal fall and winter.

Tropical North Atlantic (TNA) Index. Captures temperature anomalies in the North Atlantic region (55°W–15°W, 5°N–25°N), which influence atmospheric circulation and precipitation over the adjacent continents.

Tropical South Atlantic (TSA) Index. Analogous to the TNA, this index reflects anomalies in the South Atlantic and is used in conjunction with TNA to identify a dipolar mode of variability in the Atlantic sector[98].

Tropical Atlantic SST Gradient Index (TASI). Defined as the difference between the TNA and TSA indices, TASI captures the meridional gradient of sea surface conditions in the Atlantic, a key indicator of the Atlantic dipole mode[98].

Southwest Indian Ocean (SWIO) Index. Represents variability in the region southeast of Madagascar (31°E–45°E, 32°S–25°S), where elevated temperatures have been linked to enhanced austral summer rainfall over southern Africa[99].

Western Tropical Indian Ocean (WTIO) Index. Reflects SST variability in the western Indian Ocean (50°E–70°E, 10°S–10°N) and contributes to the Dipole Mode Index (DMI) calculated as the difference between WTIO and the southeastern Indian Ocean (SETIO: 90°E–110°E, 10°S–0°S) a key metric of the Indian Ocean Dipole[100]. High DMI values have been associated with anomalous East African rainfall[101].

Atlantic 3 (ATL3) Index. Represents SST anomalies in the equatorial Atlantic (20°W–0°, 2.5°S–2.5°N) and is used to monitor equatorial Atlantic variability based on a ± 0.4 °C threshold.

Pacific Decadal Oscillation (PDO). A low-frequency climate pattern with El Niño-like manifestations primarily in the North Pacific and North American regions.

Southern Annular Mode (SAM). Also known as the Antarctic Oscillation, the SAM index describes variations in the zonal pressure gradient between the mid-latitudes and Antarctica, influencing the climate of the Southern Hemisphere.

All climate indices were sourced from the NOAA Physical Sciences Laboratory (https://psl.noaa.gov/gcos_wgsp/Timeseries, accessed April 2025).

Steric sea level

Steric sea level variations and their components were derived from the CMEMS ARMOR-3D product (https://doi.org/10.48670/moi-00052, accessed April 2025). This dataset provides monthly temperature and salinity profiles at a spatial resolution of 0.25° × 0.25° and 50 vertical levels, covering the period 1993–2023. The fields are generated through optimal interpolation of in situ measurements (e.g., CTDs, ARGO floats, XBTs) and satellite observations and are widely recognized for robust steric sea level analyses[102].

The steric component of sea level anomalies (SSLA) is calculated using the formula[14,34,103,104]:

$$SSLA = -\int_{-H}^{0} \frac{\Delta\rho}{\rho_0} dz$$

where ρ_0 = 1025 kg/m^3 is the reference density, $\Delta\rho$ is the density anomaly with relative to the 1993–2023 climatology, and H represents the integration depth (either 700 m or the local seafloor, whichever is shallower).

Thermosteric (TSLA) and halosteric (HSLA) components were estimated separately using the TEOS-10 formulation[105–107]:

$$TSLA = \int_{-H}^{0} \alpha \Delta T dz \, , HSLA = -\int_{-H}^{0} \beta \Delta S dz$$

Here, α and β denote the thermal expansion and haline contraction coefficients, respectively, which were computed in accordance with the Thermodynamic Equation of Seawater standard[105]. The variables ΔT and ΔS are the anomalies in temperature and salinity relative to the same climatological baseline. All calculations were limited to the upper 700 m, as this layer is well-observed and captures the dominant steric signal over the LMEs' typically shallow continental shelves. Contributions below 700 m were excluded due to their minor role in interannual variability and higher uncertainty[108]. Ocean mass (Manometric sea level) changes were inferred as the residual between total SLA (from Section "Regional sea level rise and the exceptional 2023 event in Africa") and steric SLA (from this section), with the SLA field already corrected for GIA[39], and no further correction applied to the residual. To isolate non-seasonal signals, seasonal cycles (annual and semi-annual) were removed at each grid point using a least-squares fit of 12- and 6-month sinusoids. A 3-month Lanczos filter was then applied to each dataset to suppress high-frequency variability. Long-term linear trends were derived from the deseasonalized, filtered monthly time series using ordinary least squares regression[109]. Uncertainties were expressed as 95% confidence intervals (±2σ) and corrected for serial correlation[110] to ensure robust error estimates. To assess statistical significance, we used the Modified Mann–Kendall test[111], a non-parametric method that accounts for both autocorrelation and non-normality in the time series, providing a rigorous evaluation of trend reliability.

Data availability

Copernicus Marine Environment Monitoring Service (CMEMS) altimetry products are publicly available at https://doi.org/10.48670/moi-00148. The CMEMS ARMOR-3D temperature and salinity fields are available at https://doi.org/10.48670/moi-00052. AVISO Dynamic Atmospheric Correction (DAC v4.0) products can be accessed at https://tds.aviso.altimetry.fr. Climate indices (Niño 3.4, TNA, TSA, TASI, SWIO, WTIO, SETIO, DMI, ATL3, PDO, SAM) are publicly available from the NOAA Physical Sciences Laboratory at https://psl.noaa.gov/gcos_wgsp/Timeseries. The ICE6G-D

model outputs used for glacial isostatic adjustment (GIA) corrections are available from Peltier et al.[97].

Code availability

The codes[112] utilized to produce the findings in this article can be found at https://doi.org/10.5281/zenodo.17401591. The color schemes adhere to the color-blind-friendly palettes of Crameri et al.[113], and the mapping was done using the Generic Mapping Tools (GMT)[114].

Received: 14 July 2025; Accepted: 29 October 2025;
Published online: 15 December 2025

References

1. Leatherman, S. P. Social and economic costs of sea level rise. in *International Geophysics* (Elsevier, 2001).
2. Rullens, V. et al. Understanding the consequences of sea level rise: the ecological implications of losing intertidal habitat. *N. Zeal J. Mar. Freshw. Res.* **56**, 353–370 (2022).
3. WMO. State of the Global Climate 2023. (2024). https://doi.org/10.18356/9789263113474 (2025).
4. WMO. State of the Climate in Africa 2024. 7 https://doi.org/10.18356/9789263113702 (2025).
5. Cazenave, A. & Moreira, L. Contemporary sea-level changes from global to local scales: a review. *Proc. R. Soc. A* **478**, 20220049 (2022).
6. Durand, G. et al. Sea-level rise: from global perspectives to local services. *Front. Mar. Sci.* **8** https://doi.org/10.3389/fmars.2021.709595 (2022).
7. Minobe, S. et al. Global and regional drivers for exceptional climate extremes in 2023-2024: beyond the new normal. *NPJ Clim. Atmos. Sci.* **8**, 138–111 (2025).
8. Ripple, W. J. et al. The 2023 state of the climate report: entering uncharted territory. *Bioscience* **73**, 841–850 (2023).
9. Kemgang Ghomsi, F. E. et al. Sea level trends along the South African coast from 1993 to 2022 using XTRACK altimetry, tide gauges, and GNSS measurements. *Sci. Rep.* **15**, 4946–4915 (2025).
10. Kemgang Ghomsi, F. E. et al. Vertical crustal movement along the coast of South Africa. *Int. Arch. Photogramm. Remote Sens. Spat. Inf. Sci.* **48**, 393–397 (2025).
11. Trisos, C. et al. Africa. In: *Climate Change 2022: Impacts, Adaptation and Vulnerability. Contribution of Working Group II to the Sixth Assessment Report of the Intergovernmental Panel on Climate Change* (Cambridge University Press, 2023).
12. Maul, G. A., Duedall, I. W., Makowski, C. & Finkl, C. W. *Encyclopedia of Earth Sciences Series* (Springer International Publishing, 2019).
13. Aretouyap, Z., Ghomsi, F. E. K., Domra, J. K., Tchato, S. C. & Perilli, N. Assessing groundwater potential in Foumban and implication on urban planning in the context of sustainable development. *Geocarto Int.* **38** https://doi.org/10.1080/10106049.2022.2163307 (2023).
14. Ghomsi, F. E. K. et al. Exploring steric sea level variability in the Eastern Tropical Atlantic Ocean: a three-decade study (1993–2022). *Sci. Rep.* **14**, 20458 (2024).
15. Ghomsi, F. E. K. et al. Sea level rise and coastal flooding risks in the Gulf of Guinea. *Sci. Rep.* **14**, 1–11 (2024).
16. Nhantumbo, B. J., Dada, O. A. & Ghomsi, F. E. Sea level rise and climate change-impacts on African coastal systems and cities. https://doi.org/10.5772/intechopen.113083 (2023).
17. Njiiri, W., Njuguna, M. & Wahome, E. Establishing historical shoreline trends for adaption of maritime built heritage to climate change part 2: the Northern Kenya Coast. *Hist. Environ.* **16**, 167–186 (2025).
18. Chounna Yemele, G. et al. Land subsidence dynamics and their interplay with spatial and temporal land-use transitions in the Douala coastland, Cameroon. *EGUsphere* **2025**, 1–29 (2025).
19. Daramola, O. E. et al. Detection of crustal deformation using a gravimetric and Multitemporal Interferometric SAR (MT-InSAR) approach: detection of crustal deformation. *Pure Appl. Geophys.* **182**, 2111–2134 (2025).
20. Ohenhen, L. & Shirzaei, M. Land subsidence hazard and building collapse risk in the coastal city of Lagos, West Africa. *Earth's Future* **10**, e2022EF003219 (2022).
21. Magalhães Filho, L. N. L., Roebeling, P. C., Costa, L. F. C. & de Lima, L. T. Ecosystem services values at risk in the Atlantic coastal zone due to sea-level rise and socioeconomic development. *Ecosyst. Serv.* **58**, 101492 (2022).
22. Sweijd, N. A. & Smit, A. J. Trends in sea surface temperature and chlorophyll-a in the seven African large marine ecosystems. *Environ. Dev.* **36**, 100585 (2020).
23. Ibrahim, A., Salifu, A.-H. & Peprah, C. Does governance matter when disaster looms? Zooming into proactive institutional measures for flood risk management. *Int. J. Disaster Risk Reduct.* **97**, 104021 (2023).
24. Sarkodie, S. A., Ahmed, M. Y. & Owusu, P. A. Global adaptation readiness and income mitigate sectoral climate change vulnerabilities. *Human. Soc. Sci. Commun.* **9**, 1–17 (2022).
25. Bakun, A. et al. Anticipated effects of climate change on coastal upwelling ecosystems. *Curr. Clim. Change Rep.* **1**, 85–93 (2015).
26. Ramírez, F., Shannon, L. J., Angelini, R., Steenbeek, J. & Coll, M. Overfishing species on the move may burden seafood provision in the low-latitude Atlantic Ocean. *Sci. total Environ.* **836**, 155480–155480 (2022).
27. Jury, C. P. & Toonen, R. J. Widespread scope for coral adaptation under combined ocean warming and acidification. *Proc. R. Soc. B* **291**, 20241161 (2024).
28. Nurse, L. A. et al. Small islands. *Climate change 2014: Impacts, adaptation, and vulnerability. Part B: Regional aspects. Contribution of working group II to the fifth assessment report of the intergovernmental panel on climate change*, pp. 1613-1654 (2014).
29. Tamoffo, A. T., Weber, T. & Saleem, F. Population exposed to compound extreme hot & humid and wet & windy events in Africa. *Environ. Res. Lett.* **20**, 14038 (2025).
30. Didi, S. R., Diakhaté, M. & Diedhiou, A. Changes in the West Africa Monsoon precipitation extremes during ENSO developing Phases. *Atmos.-ocean* **61**, 293–305 (2023).
31. Aryee, J. N. A. et al. Quantifying climatic heavy-precipitation-induced floods in West Africa using multiple precipitation indices Quantifying climatic heavy-precipitation-induced floods in West Africa using multiple precipitation indices. *Sci. Afr.* **25**, e02309 (2024).
32. Kenfack, K. et al. Radiative anomalies associated with extreme precipitation of November 2023 in equatorial Central Africa. *Atmos. Res.* **321**, 108090 (2025).
33. Tchana, B. C. et al. Analysis of air temperature anomalies during abnormal rainfall events in Western Central Africa from September to November 2023: Analysis of air temperature anomalies during abnormal rainfall events in Western Central Africa from September to November 2023. *Theor. Appl. Climatol.* **156**, 288 (2025).
34. Ghomsi, F. E. K. et al. Sea level variability in Gulf of Guinea from satellite altimetry. *Sci. Rep.* **14**, 4759 (2024).
35. Saber, M. et al. A comprehensive review of climate change adaptation and disaster risk reduction in Africa. *J. Water Clim. change* **16**, 1831–1862 (2025).
36. Carbon, B. Analysis: Africa's extreme weather has killed at least 15,000 people in 2023. *Carbon Brief.* https://www.carbonbrief.org/analysis-africas-extreme-weather-have-killed-at-least-15000-people-in-2023/ (2023).
37. Zaine, P., Ramontsheng, R., Sarah, R. & Moagabo, R. Analysing the atmospheric-oceanic conditions driving the sustained long track and intensity of Tropical Cyclone Freddy Analysing the atmospheric-oceanic conditions driving the sustained long track and intensity of Tropical Cyclone Freddy. *Trop. Cyclone Res. Rev.* **13**, 356–388 (2024).

38. Armon, M., Shmilovitz, Y. & Dente, E. Anatomy of a foreseeable disaster: Lessons from the 2023 dam-breaching flood in Derna, Libya. *Sci. Adv.* **11**, eadu2865 (2025).
39. Cazenave, A. et al. Global sea-level budget 1993–present. *Earth Syst. Sci. Data* **10**, 1551–1590 (2018).
40. Lian, T., Wang, J., Chen, D., Liu, T. & Wang, D. A strong 2023/24 El Niño is Staged by Tropical Pacific Ocean Heat Content Buildup. *Ocean-land-atmos. Res.* **2**, 187–193 (2023).
41. Peng, Q., Xie, S.-P., Passalacqua, G. A., Miyamoto, A. & Deser, C. The 2023 extreme coastal El Niño: atmospheric and air-sea coupling mechanisms. *Sci. Adv.* **10**, eadk8646 (2024).
42. Ericson, J. P., Vörösmarty, C. J., Dingman, S. L., Ward, L. G. & Meybeck, M. Effective sea-level rise and deltas: causes of change and human dimension implications. *Glob. Planet. Change* **50**, 63–82 (2006).
43. Nicholls, R. J. Coastal flooding and wetland loss in the 21st century: changes under the SRES climate and socio-economic scenarios. *Glob. Environ. Change* **14**, 69–86 (2004).
44. Leclercq, L. et al. Spatio-temporal changes in interannual sea level along the world coastlines. *Glob. Planet. Change*, 104972 https://doi.org/10.1016/j.gloplacha.2025.104972 (2025).
45. Intergovernmental Panel on Climate, C. *Climate Change 2022 – Impacts, Adaptation and Vulnerability: Working Group II Contribution to the Sixth Assessment Report of the Intergovernmental Panel on Climate Change* (Cambridge University Press, 2023).
46. Rounce, D. R. et al. Downstream hydrology reduces glaciers' direct contribution to sea-level rise. *Geophys. Res. Lett.* **52**, e2025GL114866 https://doi.org/10.1029/2025GL114866 (2025).
47. Parkes, D. & Marzeion, B. Twentieth-century contribution to sea-level rise from uncharted glaciers. *Nature* **563**, 551–554 (2018).
48. Shi, Q., Pavey, E. S. & Carter, R. E. Bonferroni-based correction factor for multiple, correlated endpoints. *Pharm. Stat.* **11**, 300–309 (2012).
49. Hamlington, B. et al. The rate of global sea level rise doubled during the past three decades. *Commun. Earth Environ.* **5**, 601 (2024).
50. Bellas-Manley, A., Nerem, R. S. & Hamlington, B. D. Extrapolation of the Satellite Altimeter record to understand regional variations in future sea level change. *J. Geophys. Res. Oceans* **130**, e2024JC022094 https://doi.org/10.1029/2024JC022094 (2025).
51. Mitrovica, J. X. et al. On the robustness of predictions of sea level fingerprints. *Geophys. J. Int.* **187**, 729–742 (2011).
52. Dussaillant, I. et al. Annual mass change of the world's glaciers from 1976 to 2024 by temporal downscaling of satellite data with in situ observations. *Earth Syst. Sci. Data* https://doi.org/10.3929/ethz-b-000735850 (2025).
53. von Schuckmann, K. et al. Heat stored in the Earth system 1960–2020: where does the energy go? *Earth Syst. Sci. Data* **15**, 1675–1709 (2023).
54. Pörtner, H.-O. et al. The ocean and cryosphere in a changing climate. *IPCC special report on the ocean and cryosphere in a changing climate. Cambridge University Press* **1155** https://doi.org/10.1017/9781009157964 (2019).
55. Intergovernmental Panel on Climate Change (IPCC) (Ed.). Climate Change 2022—Mitigation of Climate Change https://doi.org/10.1017/9781009157926 (2023).
56. Spalding, M. D. et al. Coastal ecosystems: a critical element of risk reduction. *Conserv. Lett.* **7**, 293–301 (2014).
57. Frederikse, T. et al. The causes of sea-level rise since 1900. *Nature* **584**, 393–397 (2020).
58. Syvitski, J. P. M. et al. Sinking deltas due to human activities. *Nat. Geosci.* **2**, 681–686 (2009).
59. Hutchings, L. et al. The Benguela current: an ecosystem of four components. *Prog. Oceanogr.* **83**, 15–32 (2009).
60. Durgadoo, J. V., Rühs, S., Biastoch, A. & Böning, C. W. B. Indian Ocean sources of Agulhas leakage. *J. Geophys. Res. Oceans* **122**, 3481–3499 (2017).
61. Llovel, W. et al. Global ocean freshening, ocean mass increase and global mean sea level rise over 2005–2015. *Sci. Rep.* **9**, 17717 (2019).
62. Zemp, M. et al. Community estimate of global glacier mass changes from 2000 to 2023. *Nature* **639**, 382–388 (2025).
63. Swapna, P., Jyoti, J., Krishnan, R., Sandeep, N. & Griffies, S. M. Multidecadal weakening of indian summer monsoon circulation induces an increasing Northern Indian Ocean Sea Level. *Geophys. Res. Lett.* **44**, 10,560–510,572 (2017).
64. Chatterjee, A., Kumar, B. P., Prakash, S. & Singh, P. Annihilation of the Somali upwelling system during summer monsoon. *Sci. Rep.* **9**, 7598–7598 (2019).
65. Stüwe, K., Robl, J., Turab, S. A., Sternai, P. & Stuart, F. M. Feedbacks between sea-floor spreading, trade winds and precipitation in the Southern Red Sea. *Nat. Commun.* **13**, 5405–5405 (2022).
66. Bonaduce, A., Pinardi, N., Oddo, P., Spada, G. & Larnicol, G. Sea-level variability in the Mediterranean Sea from altimetry and tide gauges. *Clim. Dyn.* **47**, 2851–2866 (2016).
67. Legeais, J.-F. et al. An improved and homogeneous altimeter sea level record from the ESA Climate Change Initiative. *Earth Syst. Sci. Data* **10**, 281–301 (2018).
68. Marcos, M. & Tsimplis, M. N. Coastal sea level trends in Southern Europe. *Geophys. J. Int.* **175**, 70–82 (2008).
69. Borile, F. et al. The Eastern Mediterranean Sea mean sea level decadal slowdown: the effects of the water budget. *Front. Clim.* **7** https://doi.org/10.3389/fclim.2025.1472731 (2025).
70. Durack, P. J., Wijffels, S. E. & Matear, R. J. Ocean salinities reveal strong global water cycle intensification during 1950 to 2000. *Science* **336**, 455–458 (2012).
71. Han, W. et al. Spatial patterns of sea level variability associated with natural internal climate modes. *Surv. Geophys.* **38**, 217–250 (2017).
72. Zhang, X. & Church, J. A. Sea level trends, interannual and decadal variability in the Pacific Ocean. *Geophys. Res. Lett.* **39**, L21701 (2012).
73. Meehl, G. A. et al. Atlantic and Pacific tropics connected by mutually interactive decadal-timescale processes. *Nat. Geosci.* **14**, 36–42 (2021).
74. Boening, C., Willis, J. K., Landerer, F. W., Nerem, R. S. & Fasullo, J. The 2011 La Niña: so strong, the oceans fell. *Geophys. Res. Lett.* **39**, L19602 (2012).
75. Forster, P. M. et al. Indicators of Global Climate Change 2023: annual update of key indicators of the state of the climate system and human influence. *Earth Syst. Sci. Data* **16**, 2625–2658 (2024).
76. Bevacqua, E., Schleussner, C.-F. & Zscheischler, J. A year above 1.5 °C signals that Earth is most probably within the 20-year period that will reach the Paris Agreement limit. *Nat. Clim. change* **15**, 262–265 (2025).
77. Schaeffer, R., Gustafsson, Ö., Riipinen, I. & Ziervogel, G. Ten new insights in climate science 2024. *One Earth* https://doi.org/10.1016/j.oneear.2025.101285 (2025).
78. Li, Z., England, M. H. & Groeskamp, S. Recent acceleration in global ocean heat accumulation by mode and intermediate waters. *Nat. Commun.* **14**, 6888–6814 (2023).
79. Cheng, L. et al. Record high temperatures in the Ocean in 2024. *Adv. Atmos. Sci.* **42**, 1092–1109 (2025).
80. Huang, B. et al. Extreme marine heatwaves in the global oceans during the past decade. *Bull. Am. Meteorol. Soc.*https://doi.org/10.1175/BAMS-D-24-0337.1 (2025).
81. Nicholls, R. J. et al. A global analysis of subsidence, relative sea-level change and coastal flood exposure. *Nat. Clim. Change* **11**, 338–342 (2021).

82. Hakuba, M. Z. et al. Trends and Variability in Earth's energy imbalance and ocean heat uptake since 2005. *Surv. Geophys.* **45**, 1721–1756 (2024).
83. Jiang, N. et al. El Niño and sea surface temperature pattern effects lead to historically high global mean surface temperatures in 2023. *Geophys. Res. Lett.* **52**, e2024GL113733 https://doi.org/10.1029/2024GL113733 (2025).
84. Matano, R. P. & Palma, E. D. On the upwelling of downwelling currents. *J. Phys. Oceanogr.* **38**, 2482–2500 (2008).
85. Swart, N. C., Lutjeharms, J. R. E., Ridderinkhof, H. & de Ruijter, W. P. M. Observed characteristics of Mozambique Channel eddies. *J. Geophys. Res. Atmos.* **115** https://doi.org/10.1029/2009JC005875 (2010).
86. Fox-Kemper, B. H. et al. *2021: The Physical Science Basis*. *Contribution of Working Group I to the Sixth Assessment Report of the Intergovernmental Panel on Climate Change* (eds Zhai Masson-Delmotte, P. et al.) 1211–1362 (Cambridge University Press, 2021).
87. Gunnarson, J. L. et al. Removing ENSO's influence from global SST variability, with insights into the record-setting marine heatwaves of 2023-2024. *Bull. Am. Meteorol. Soc.* https://doi.org/10.1175/BAMS-D-24-0023.1 (2025).
88. Jarugula, S. & McPhaden, M. J. Indian Ocean Dipole affects eastern tropical Atlantic salinity through Congo River Basin hydrology. *Commun. Earth Environ.* **4**, 366–369 (2023).
89. West Africa Seasonal, M. 2023 Season – August Update. (https://reliefweb.int/attachments/5a81cb98-60b6-4c00-a60d-751bb3d62cd3/WFP-0000151903.pdf, 2023).
90. Cai, W. et al. Climate impacts of the El Niño–Southern Oscillation in Africa. *Nat. Rev. Earth Environ.* **6**, 503–520 (2025).
91. United Nations Human Settlements, P. *State of the world's cities, 2008/2009: harmonious cities*. (2008).
92. Bindoff, N. L. et al. Changing ocean, marine ecosystems, and dependent communities. *Intergovernmental Panel on Climate Change (IPCC), Intergovernmental Panel* https://doi.org/10.1017/9781009157964.007 (2022).
93. García-Reyes, M. et al. Under Pressure: Climate Change, Upwelling, and Eastern Boundary Upwelling Ecosystems. *Front. Mar. Sci.* **2** https://doi.org/10.3389/fmars.2015.00109 (2015).
94. Dubois, K., Larsen, M. A. D., Drews, M., Nilsson, E. & Rutgersson, A. Influence of data source and copula statistics on estimates of compound flood extremes in a river mouth environment. *Nat. Hazards Earth Syst. Sci.* **24**, 3245–3265 (2024).
95. Landerer, F. W. & Volkov, D. L. The anatomy of recent large sea level fluctuations in the Mediterranean Sea. *Geophys. Res. Lett.* **40**, 553–557 (2013).
96. Ablain, M. et al. The TOPEX-A drift and impacts on GMSL time series Comparison with Poseïdon, p. 2017, https://meetings.aviso.altimetry.fr/fileadmin/user_ upload/tx_ausyclsseminar/files/Poster_OSTST17_GMSL_ Drift_TOPEX-A.pdf (2017). (last access: 2 November 2022).
97. Peltier, W. R., Argus, D. F. & Drummond, R. Comment on "An assessment of the ICE-6G_C (VM5a) glacial isostatic adjustment model" by Purcell et al. *J. Geophys. Res. Solid Earth* **123**, 2019–2028 (2018).
98. Enfield, D. B., Mestas-Nuñez, A. M. & Trimble, P. J. The Atlantic multidecadal oscillation and its relation to rainfall and river flows in the continental US. *Geophys. Res. Lett.* **28**, 2077–2080 (2001).
99. Hermes, J. C. & Reason, C. J. C. Ocean model diagnosis of interannual coevolving SST variability in the South Indian and South Atlantic Oceans. *J. Clim.* **18**, 2864–2882 (2005).
100. Saji, N., Goswami, B. N., Vinayachandran, P. & Yamagata, T. A dipole mode in the tropical Indian Ocean. *Nature* **401**, 360–363 (1999).
101. Black, E., Laughton, A. S., Flemming, N. C. & Spencer, T. The relationship between Indian Ocean sea–surface temperature and East African rainfall. *Philos. Trans. R. Soc. Lond. Ser. A: Math. Phys. Eng. Sci.* **363**, 43–47 (2005).
102. Gasparin, F. et al. Requirements for an integrated in situ Atlantic Ocean observing system from coordinated observing system simulation experiments. *Front. Mar. Sci.* **6** https://doi.org/10.3389/fmars.2019.00083 (2019).
103. Siegismund, F., Johannessen, J., Drange, H., Mork, K. A. & Korablev, A. Steric height variability in the Nordic Seas. *J. Geophys. Res. C. Oceans* **112**, n/a https://doi.org/10.1029/2007JC004221 (2007).
104. Piecuch, C. G. & Ponte, R. M. Mechanisms of Global-mean steric sea level change. *J. Clim.* **27**, 824–834 (2014).
105. Pawlowicz, R. & Feistel, R. Limnological applications of the Thermodynamic Equation of Seawater 2010 (TEOS-10). *Limnol. Oceanogr. Methods* **10**, 853–867 (2012).
106. Jayne, S. R., Wahr, J. M. & Bryan, F. O. Observing ocean heat content using satellite gravity and altimetry. *J. Geophys. Res. C. Oceans* **108**, 13.11-n/a https://doi.org/10.1029/2002JC001619 (2003).
107. Wang, G., Cheng, L., Boyer, T. & Li, C. Halosteric sea level changes during the Argo era. *Water* **9**, 484 (2017).
108. Purkey, S. G. & Johnson, G. C. Warming of Global Abyssal and Deep Southern Ocean Waters between the 1990s and 2000s: contributions to global heat and sea level rise budgets. *J. Clim.* **23**, 6336–6351 (2010).
109. Wooditch, A., Johnson, N. J., Solymosi, R., Medina Ariza, J. & Langton, S. *Ordinary Least Squares Regression* (Springer International Publishing, 2021).
110. Emery, W. J., Talley, L. D. & Pickard, G. L. Descriptive physical oceanography. *available at: HTU* http://www-pord.ucsd.edu/~ltalley/sio210/pickard_emery/UT (2006).
111. Alashan, S. Combination of modified Mann-Kendall method and Şen innovative trend analysis. *Engineering Rep.* **2**, n/a https://doi.org/10.1002/eng2.12131 (2020).
112. Ghomsi, F. E. K., Stroeve, J., Bonaduce, A. & Raj, R. P. Accelerating sea level rise in Africa and its large marine ecosystems since the 1990s. *Zenodo*. https://doi.org/10.5281/zenodo.17401590 (2025).
113. Crameri, F., Shephard, G. & Heron, P. J. Choosing suitable color palettes for accessible and accurate science figures. https://doi.org/10.1002/cpz1.1126 (2024).
114. Wessel, P. et al. The generic mapping tools version 6. *Geochem. Geophys. Geosyst.* **20**, 5556–5564 (2019).

Acknowledgements

F.E.K.G. and J.S. acknowledge funding from Canada's C150 Research Program (Grant No. 50296). F.E.K.G., R.P.R., and A.B. are supported by the Sea Level Predictions and Reconstructions (SeaPR) project, funded through the Bjerknes Centre for Climate Research (BCCR) Strategic Projects Initiative. F.E.K.G received support from Schmidt Sciences, LLC. R.P.R. and A.B. also acknowledge support from the European Space Agency's DRAGON 5 project. We are grateful to the three anonymous reviewers, the Editorial Board Member, and the Deputy Editor for their thoughtful and constructive feedback, which greatly improved this work.

Author contributions

F.E.K.G. conceived the study, led the analysis, and developed the methodology, software, and visualizations. J.S. contributed to the methodology, validation, and provided overall supervision. A.B. and R.P.R. assisted with methodological development and validation. Project management was jointly carried out by F.E.K.G. and J.S. F.E.K.G. drafted the manuscript, and all authors contributed to its revision and approved the final version.

Competing interests

The authors declare no competing interests.

Additional information

Supplementary information The online version contains supplementary material available at https://doi.org/10.1038/s43247-025-02965-z.

Correspondence and requests for materials should be addressed to Franck Eitel Kemgang Ghomsi.

Peer review information *Communications Earth & Environment* thanks the anonymous reviewers for their contribution to the peer review of this work. Primary Handling Editors: Olusegun Dada, Joe Aslin and Alice Drinkwater. A peer review file is available.